



universität
wien

MASTERARBEIT

Titel der Masterarbeit

„Molecular Droplets Coupled to Intense Cavity Fields“

Verfasser

Stefan Kuhn, BSc

angestrebter akademischer Grad

Master of Science (MSc)

Wien, 2013

Studienkennzahl lt. Studienblatt:

A 066 876

Studienrichtung lt. Studienblatt:

Masterstudium Physik UG2002

Betreuerin / Betreuer:

Prof. Dr. Markus Arndt

Contents

1	Introduction	9
2	Principles of cavity cooling methods for dielectric nano-particles	13
2.1	Radial cooling of a point-like polarizable particle	13
2.2	Effects for extended particles	19
3	Experimental Set-up	23
3.1	Cavity design	24
3.2	Pumping and stabilising the cavity	25
3.2.1	Pumping the fundamental mode	25
3.2.2	Pumping a higher-order TEM mode	26
3.2.3	Stabilisation of the cavity	28
3.3	Particle source	30
3.4	Detection of the cavity and particle dynamics	31
3.4.1	Transmitted intensity through the fundamental cavity mode . . .	32
3.4.2	Phase and amplitude of TEM ₀₀ & TEM ₁₁ modes	32
3.4.3	Scattered light	35
4	Results	37
4.1	Detection of a droplet passing through the cavity mode	38
4.2	Channelling of a droplet through the standing wave	41
4.3	Cavity induced turning back of a droplet	43
4.4	Effective low-field seeking behaviour	46
4.5	Asymmetries in the scattered light	48
4.6	Sudden changes in the scattering behaviour	50
4.7	Thermal feedback	50
5	Conclusion & Outlook	55

Contents

6	Supplements	59
6.1	Molecules	59
6.2	Extracting phase and amplitude of the TEM_{00} & TEM_{11} mode from the digitized beating signal	60
6.3	Reconstruction of the trajectory for a particle trapped in the standing wave	62

Danksagung

Zuallererst möchte ich mich bei meinem Betreuer Prof. Dr. Markus Arndt bedanken, dass er mir ermöglicht hat, in seiner Forschungsgruppe mitarbeiten zu dürfen und mich dabei bestmöglich unterstützt hat.

Des Weiteren bedanke ich mich bei Peter Asenbaum, der mich mit dem Experiment vertraut gemacht hat und von dem ich viel lernen durfte. Außerdem möchte ich mich bei ihm für das Korrekturlesen meiner Thesis bedanken.

Darüber hinaus möchte ich mich bei der gesamten Quantennano-Gruppe und auch bei meinen beiden Büro-Kollegen bedanken. Es ist ein Vergnügen gemeinsam mit Euch arbeiten zu dürfen.

Ein besonderer Dank gilt vor allem meiner Familie, die es mir überhaupt erst ermöglicht hat, mein Studium in dieser Form ausüben zu können und stets ein wesentlicher Rückhalt war.

Schlussendlich seien hier auch meine Freunde erwähnt, die mich nach langen Labortagen ertragen und mich auch auf andere Gedanken gebracht haben.

Abstract

Future quantum experiments with neutral nano-particles will require long interaction and coherence times. Therefore, cold and slow particles are needed. These demands can not be covered by current sources for launching objects of the desired masses. Thus, schemes for controlling their motion need to be established. We present a new experimental set-up that aims at the detection and characterisation of large molecular droplets. It is designed in order to show first manipulation effects and to lead a way towards a regime in which cavity cooling is feasible.

Intense infrared fields (1560 nm) in a high-finesse cavity can be used to slow/cool the particle motion. Since the off-resonant coupling to the optical field is mediated by the induced electric dipole moment, this method can, in principle, be applied to every polarizable particle - with increasing efficiency for objects of growing size up to a length scale comparable to a fraction of the infrared wavelength. We have, however, also performed experimental and theoretical studies for droplets beyond this limit.

The high finesse resonator also permits to track the passage of molecular droplets and details of their motion through the field modes. In order to obtain more specific information, in addition to the strongly pumped fundamental resonator mode, we couple a higher order transverse mode into the cavity and monitor its interaction with the nano-particles.

Within this thesis I present our set-up and show first experimental results: In a laser evaporation scheme we produce nano- and micrometer sized droplets made of organic molecules, which were synthesized in the group of Prof. M. Mayor in Basel in order to meet the demands of interferometric experiments with molecules. We discuss first manipulation effects for these droplets, containing amongst others the reconstruction of a particle motion from the variety of signals obtained in our set-up via a computer simulation. Furthermore we will present a cavity induced turning back of a droplet. Finally, we are going to discuss the limitations for the current experiments and the prospects for slowing and cooling of mesoscopic particles in a future set-up.

Zusammenfassung

Die Anforderungen für zukünftige Quantenexperimente liegen weitestgehend darin, Quellen für langsame und kalte Nanoteilchen zu entwickeln, um lange Wechselwirkungs- und Kohärenzzeiten zu erreichen. In dieser Arbeit präsentieren wir einen experimentellen Aufbau, der mit dem Ziel entworfen wurde, Molekültröpfchen mittels optischer Kräfte zu kühlen. Intensive Infrarotfelder (1560nm), abseits der Molekülresonanzen, können in einem optischen Resonator derart überhöht werden, dass die wirkenden Kräfte ausreichen, um die Bewegungen der Teilchen zu beeinflussen und zu bremsen bzw. zu kühlen. Da dieser Effekt auf der Wechselwirkung zwischen dem elektromagnetischen Feld und dem im Teilchen induzierten Dipolmoment basiert, kann dieses Schema auf polarisierbare Objekte jeglicher Art angewandt werden. Zudem skaliert die Effizienz dieses Vorgangs mit dem Volumen der Teilchen bishin zu einer Größe, die im Bereich der halben Wellenlänge des Infrarot-Feldes liegt. Effekte, die ab dieser Größenordnung auftreten, werden wir daher sowohl theoretisch, als auch experimentell behandeln.

Darüber hinaus ermöglicht der Resonator die Trajektorien der Teilchen nachzuverfolgen. Zu diesem Zweck wird neben der fundamentalen Resonatormode, die für das Kühlen zuständig ist, eine Transversalmode höherer Ordnung angeregt und deren Wechselwirkung mit den Teilchen beobachtet.

Im Laufe dieser Arbeit werden erste experimentelle Ergebnisse präsentiert, die nahelegen, dass das optische Manipulieren von Nanoteilchen in Reichweite liegt. Dazu betrachten wir die Bildung von Molekültröpfchen (Durchmesser 10 nm - 10 μ m) in einem Laserdesorptions-Verfahren. Wir verwenden Moleküle, die in Basel in der Gruppe von Prof. M. Mayor synthetisiert wurden, um den Anforderungen der Molekülinterferometrie-Experimente zu genügen. Dabei beobachten wir u.a. ein Teilchen, das aufgrund der Wechselwirkung mit dem Feld im Resonator beim Durchflug zum Umkehren gebracht wird. Des Weiteren wird gezeigt, wie mit Hilfe einer Computersimulation die Bewegung eines Tröpfchens durch das Lichtfeld rekonstruiert werden kann. Schlussendlich werden wir die Beschränkungen des bisherigen Aufbaus, sowie die weiteren Aussichten zum Bremsen und Kühlen von mesoskopischen Teilchen in möglichen Erweiterungen des Experiments diskutieren.

1 Introduction

In recent years, the demand for cold and slow mesoscopic particles has turned out to be a key issue for future quantum experiments [1]. They aim at testing the limits of quantum mechanics predicted by spontaneous localization theories [2–6], studying the conflict between general relativity and quantum mechanics by searching for non-Newtonian gravity forces at small scales [7], performing quantum metrology for polar or polarizable organic molecules [8] and showing quantum effects with large organic molecules up to organisms e.g. viruses [9, 10]. Experiments of these kinds require objects in the mass range of 10^7 amu to 10^{12} amu, which are mass-selected, slow, internally cold and provide a way for manipulating them in an interferometer. In the following we will focus on their translational energy. Since the existing sources for launching particles of this mass range do not yet meet the requirements given by these experiments, methods for controlling their motion need to be established.

A variety of laser cooling techniques has been developed for atoms throughout the last thirty years leading to great advance in the field of atomic physics. These methods range from Doppler cooling [11, 12] over polarization gradient cooling [13] to sub-recoil laser cooling [14, 15]. However, they require optically addressable cycling transitions. Although laser cooling has been recently demonstrated for a diatomic molecule [16], laser cooling techniques for complex molecules and nanoparticles are much more demanding. Due to their variety of rotational and vibrational degrees of freedom in addition to their electronic spectrum, closed cooling cycles do not exist for these systems. Thus, laser cooling of mesoscopic particles seems very hard to achieve.

In contrast to that, a new control scheme may overcome this problem, since it is based on the dipole force that can be exerted on a polarizable nanoparticle by off resonant light. Nevertheless, since this force is substantially weaker than in the resonant case, one has to deal with far more intense light fields. Additionally, in order to obtain a cooling mechanism for the motional energy of a mesoscopic object, a velocity-dependent friction force is required. For laser cooling of atoms this is obtained by the Doppler shift of the laser light that is coupled to the electronic transitions. For off-resonant cooling techniques it may be replaced in two different approaches:

1 Introduction

On the one hand, parametric feedback can be applied, which actively reacts onto the position of a particle trapped by the gradient force in an optical tweezer. Its scattered light is detected and reveals information about the particle position. In response to that the intensity of the trapping beam can be switched accordingly such that the motion of the particle can be cooled.

This cooling scheme has been successfully realised in two recent experiments: 3 μm -diameter SiO_2 microspheres have been trapped at pressure below 1×10^{-5} mbar and cooled to a temperature of about 1.5 mK in the group of M. Raizen [7]. In the team of L. Novotny a 140 nm-diameter fused silica nanoparticle has been cooled 3-dimensionally to about 50 mK at pressure of about 1×10^{-5} mbar [17].

On the other hand, the lack of internal cycling transitions can be replaced by external resonances of an optical field inside a high-finesse cavity. In comparison with active feedback-cooling, cavity cooling is solely based on a self-induced, time-delayed reaction of the cavity field onto the particles' position. Hence it does not require external modifications of the field dynamics.

Cavity cooling was first proposed by the group of H. Ritsch [18] and theoretically developed in other teams [19–22]. It was successfully realised experimentally for atoms [23–26] and atomic ensembles [27]. Most recently first signs of cavity cooling have been observed for a nanosphere trapped in a buffer-gas assisted dipole trap [28].

This thesis starts with introducing the basic theory behind cavity cooling. We will discuss how the motion of a mesoscopic particle can be tracked and manipulated while it transits a resonator mode. We will present the experimental set-up together with first measured results, which demonstrate the detection and characterisation of molecular droplets in a high finesse cavity and show first results indicating that cavity-cooling methods under high vacuum conditions are within reach.

Within chapter 2 we will discuss the key principles of cavity cooling for damping the radial motion of a polarizable particle flying freely through a resonator. The description is based on the most fundamental work on off-resonant cavity cooling by P. Horak et al. published in 1997 [18] and a recent proposal by P. Barker for cooling the radial components of the center-of-mass motion of a trapped nanoparticle [29].

Initially, we will focus on objects that can be approximated as point-like and therefore be treated as dipole scatterers. In a further step we will discuss additional effects that appear for nano-spheres with diameters comparable to the optical wavelength. In this regime even particles that are intrinsically attracted to higher light fields can turn into effective low-field seekers.

In chapter 3 we will focus on the experimental set-up that was designed to show first

cavity-induced manipulation effects on polarizable nano-droplets. These particles are produced using a laser evaporation technique, which will be characterised in detail. We will further discuss our detection scheme that allows us to track the motion of the particles through the resonator. Furthermore, we are able to extract the phase shift imprinted on the fundamental mode of the cavity by a droplet passing through and discuss how this effect can be related to the particles' polarizability. Additionally we will show how a higher order transversal electro-magnetic (TEM) mode provides further details about the trajectories the droplets take through the resonator. The techniques utilized for this purpose are similar to the ones used in experiments, which were carried out with atoms in the groups of H. J. Kimble and G. Rempe [30–32] respectively.

Subsequently we will examine the experimental results in chapter 4 and discuss several types of particle behaviour, which we were able to observe for droplets ...

- ... flying through the resonator, in order to demonstrate how the detected signals can be utilized for reconstructing the particle trajectory. The experimental data is complemented by a computer simulation which allows us to extract the polarizability of the droplet via the phase shift of the cavity mode.
- ... being trapped and thus channelled through an anti-node of the standing wave field. For one particular particle we will reconstruct its trajectory in the direction of the cavity based on its scattered light and investigate whether the conditions for cooling along this axis are fulfilled.
- ... showing a cavity induced turning back caused by the dynamics of the cavity field.
- ... that show an effective low-field seeking behaviour.
- ... with an unexpected asymmetry in their scattered light which seems not to be caused by cooling effects.
- ... that change their scattering behaviour while they pass through the cavity center.

At the end of chapter 4 we will discuss a thermal feedback effect which is caused by local deformations of the mirror surface on the scale of a few ångström.

Finally, we will present a short outlook and ideas for future experiments towards cavity cooling of nano-particles.

2 Principles of cavity cooling methods for dielectric nano-particles

In this chapter we want to present the basic principles of cavity-cooling for polarizable particles transiting a single mode optical cavity. First, we will motivate the field dynamics for an empty, driven resonator. Then we will let a point-like particle fly through and look at the interaction between the cavity field and the particle motion. For a better understanding of the system we will present a simulated trajectory for a particle which is trapped radially and cooled.

Finally, we will discuss effects that appear for big particles which can no longer be treated in a point-like approximation.

2.1 Radial cooling of a point-like polarizable particle

Dynamics of an empty, driven cavity

We now look at the system shown in figure 2.1. A strong pump laser field with angular frequency ω_p drives a single mode cavity with a pump rate of η . Its detuning from the cavity resonance ω_c is given by $\Delta = \omega_p - \omega_c$. Therefore, an intra-cavity field with amplitude $a(t)$ builds up, where $|a|^2$ is the total number of photons inside the resonator. Its dynamics is described by the differential equation¹

$$\dot{a}(t) = (-\kappa + i\Delta) a(t) + \eta. \quad (2.1)$$

The loss term κ accounts for the light leaking out of the resonator through the mirrors. It corresponds to the linewidth of the cavity and is of the order of a few hundred kHz. We further assume that only the TEM₀₀ mode is pumped by the driving field and interacts with the particle.

¹This expression can be derived from the Maxwell equations by additionally using the slowly envelope approximation, which is a valid assumption since the cavity dynamics are about nine orders of magnitude slower than the frequency of the pump field [22].

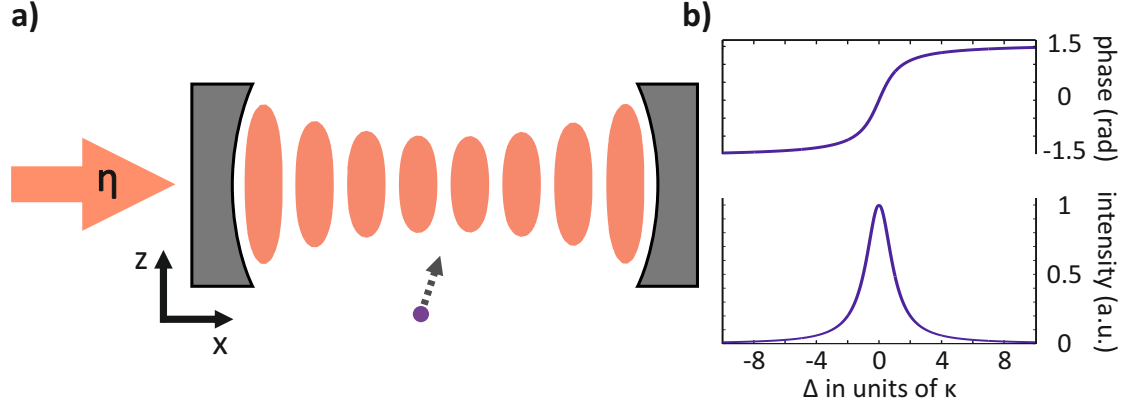


Figure 2.1: a) Schematic representation of a particle passing through a pumped single-mode cavity. The phase and intensity of the empty cavity field are plotted as a function of the detuning $\Delta = \omega_p - \omega_c$ in b).

When the pump field is switched on, it takes the cavity a time of $t \gg \frac{1}{\kappa}$ such that the mode reaches a steady state field

$$a_{ss} = \frac{\eta}{\kappa - i\Delta} \quad (2.2)$$

with a total photon number of

$$|a_{ss}|^2 = \frac{|\eta|^2}{\kappa^2 + \Delta^2} \quad (2.3)$$

which is proportional to the intra-cavity intensity. The profile of the light that is transmitted through the cavity has a Lorentzian shape as a function of the detuning Δ . It is plotted in figure 2.1 b) together with the corresponding phase of the cavity field. The latter is given by the argument of the complex field amplitude.

Coupling of a dielectric point-like particle to the cavity

Now, we let a particle fly through the cavity and couple to its mode. For the moment, we assume the particle to be point-like with a polarizability α and mass m . We further assume it to be non-absorbing but scattering in free space with rate γ_{sc} , which scales² with α^2 .

The polarizability describes the particle's interaction with the electric field inside the

²For a non-point-like particle this statement is only valid in an approximation up to the first order.

2.1 Radial cooling of a point-like polarizable particle

cavity. It is related to the particle's permittivity ϵ by the Clausius-Mossotti relation [33]

$$\alpha = 4\pi\epsilon_0 R^3 \frac{\epsilon - 1}{\epsilon + 2}. \quad (2.4)$$

A polarizable particle that maximally couples to a cavity mode therefore shifts its resonance with the coupling frequency

$$U_0 = -\frac{\alpha\omega_p}{2\epsilon_0 V} \quad (2.5)$$

by effectively changing the refractive index inside the resonator [22]. This results in an increased length of the cavity. In this expression, ϵ_0 denotes the vacuum permittivity and V the mode-volume, which is obtained by integrating the absolute square of the mode function $|f(\mathbf{x})|^2$ over the whole cavity length d . In Cartesian coordinates the mode function of the fundamental mode with waist $w(x)$ writes

$$f(\mathbf{x}) = \sin(kx) e^{-\frac{y^2+z^2}{w(x)^2}}. \quad (2.6)$$

Since we are looking at a particle that passes through the resonator, the effective coupling frequency depends on its position $\mathbf{x}(t)$ and can be expressed by

$$U(\mathbf{x}(t)) = U_0 |f(\mathbf{x}(t))|^2. \quad (2.7)$$

This expression relates to the particle's potential energy V_{opt} in the resonator via

$$V_{opt}(\mathbf{x}) = \hbar U(\mathbf{x}) |a|^2. \quad (2.8)$$

The dynamics of the driven cavity field with a polarizable point-particle coupling to it writes

$$\dot{a}(t) = [-\kappa + i\Delta - iU(\mathbf{x}(t)) - \gamma_{sc}(\mathbf{x})] a(t) + \eta. \quad (2.9)$$

In order to understand how this dynamics can lead to cooling of the radial motion inside the cavity we express the particle's position $\mathbf{x}(t)$ in cylindrical coordinates

$$x(t) = x(t) \quad (2.10)$$

$$y(t) = r(t) \cos(\phi(t)) \quad (2.11)$$

$$z(t) = r(t) \sin(\phi(t)). \quad (2.12)$$

2 Principles of cavity cooling methods for dielectric nano-particles

Now the mode function can be expressed in terms of x and r

$$f(x, r) = \sin(kx) \cdot e^{-\frac{r^2}{w^2}}. \quad (2.13)$$

The radial force on the particle is given by the dipole force $\mathbf{F} = -\nabla V_{opt}(r)$, which results from the coupling to the Gaussian part of the mode function. For a particle that enters the cavity off-centred the equations of motion write

$$\frac{d^2 r}{dt^2} = \frac{4\hbar k}{m} U_0 |a|^2 \frac{r}{w^2} e^{-\frac{2r^2}{w^2}} + \frac{L^2}{m^2 r^3} \quad (2.14)$$

$$\frac{d\phi}{dt} = \frac{L}{mr^2}. \quad (2.15)$$

Here, $L = v_0 \cdot b \cdot m$ denotes the angular momentum for a particle with initial velocity v_0 and impact parameter b with respect to the cavity center.

Since the field dynamics depends on the position of the particle in the cavity, equations 2.9, 2.14 & 2.15 are coupled. This results in a non-linear response of the intra-cavity intensity to the motion of the particle through the resonator. It can be used for cooling its translational energy in the following way:

As depicted in figure 2.2, the laser needs to be red-detuned with respect to the cavity ($\Delta < 0$). In this way, when the particle enters the resonator mode, it shifts the cavity phase towards resonance and gradually turns on the intra-cavity intensity. Since this takes place in a time delayed way, the photon number inside the resonator is still increasing after the particle has already crossed the cavity center. Consequently, the particle then has to climb a higher potential hill than it has fallen down before. The resulting difference in kinetic energy is transferred to the optical field, which provides a dissipative channel as it leaks out of the cavity. Both the evolution of the potential and the kinetic energy of the particle are plotted in figure 2.3.

In our experiments the detuning is set to be $\Delta = -\kappa$ since in this case the field intensity reacts maximally to a change in cavity phase.

By these means one can - in principle - sufficiently damp the radial part of a particle's velocity such that it gets trapped and orbits around the cavity center. In this case, the particle keeps interacting with the cavity mode and can be cooled further. When the radial part of its velocity is damped, the particle remains circling around the cavity center at a fixed radius given by its rotational energy. The latter is determined by the particle's initial angular momentum. This motion cannot be cooled in this system due to the rotational isotropy of the cavity field with just the fundamental mode being pumped.

2.1 Radial cooling of a point-like polarizable particle

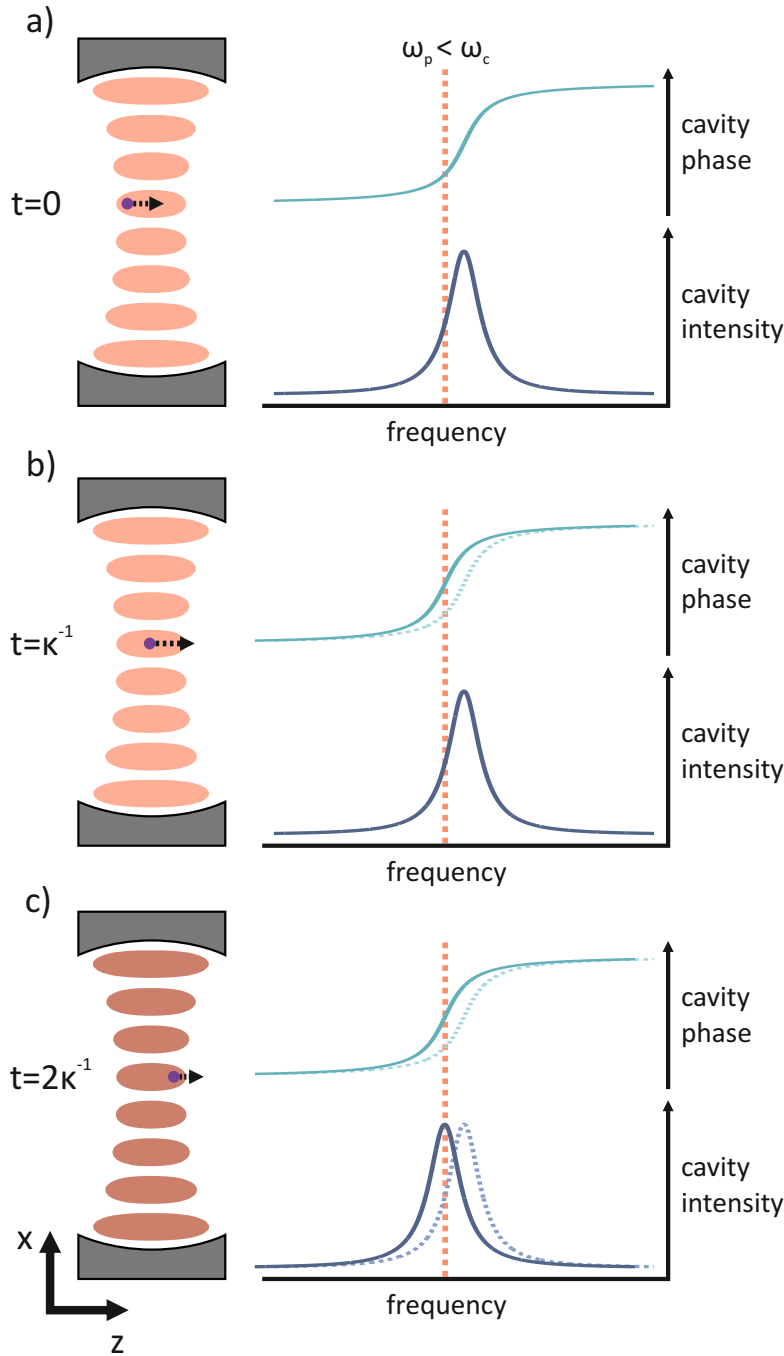


Figure 2.2: a) A particle enters the cavity mode and gets accelerated by the dipole force. b) While the particle approaches the center of the mode, the cavity phase reacts onto the particle's polarizability in a time delayed way. c) When the particle leaves the resonator again, the intra-cavity intensity reacts onto the phase shift. In this way, more light is coupled into the mode and thus the particle gets more decelerated by the dipole force than it was accelerated in the beginning.

2 Principles of cavity cooling methods for dielectric nano-particles

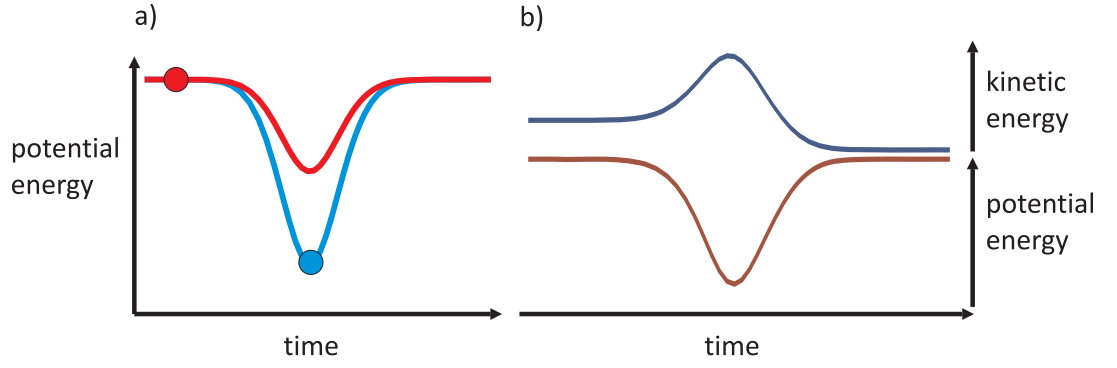


Figure 2.3: Evolution of the potential and kinetic energy of a particle, which gets cooled by the cavity. Schematically this takes place as depicted in a). When the particle enters the resonator mode it shifts the detuned cavity towards resonance and allows more light to be coupled in. Since this takes place in a time delayed way, the intra-cavity intensity is still rising while the particle has already passed through the cavity center. It thus has to climb a higher potential hill (blue) than it has fallen down before (red) and loses kinetic energy. This can be observed in b), where the dynamic evolution of both the potential and the kinetic energy for a slowed particle is depicted.

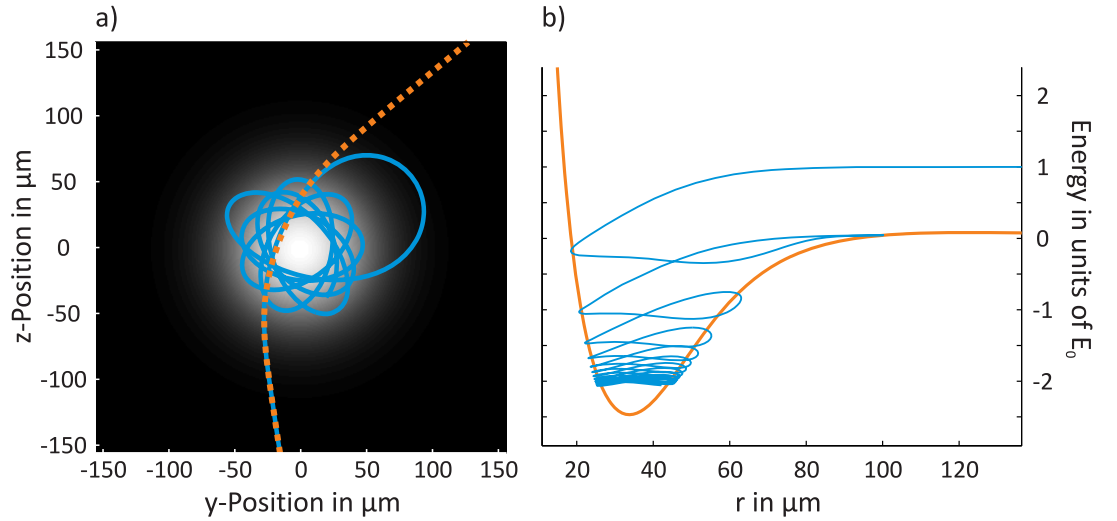


Figure 2.4: a) Blue: Simulated trajectory in the x-y-plane for a particle ($U_0 = -1.5\kappa$, $m = 4 \times 10^{10}$ amu) that gets trapped by the fundamental cavity mode (pump power 4 W), which is depicted by the black & white background. Orange: Trajectory that the particle would take if the system was behaving adiabatically. b) Energy diagram for the trapped particle (blue) in units of its initial energy E_0 . One can see that it gets cavity cooled cycle by cycle. The orange curve depicts the adiabatic potential of the cavity field.

Figure 2.4 a) shows a simulated trajectory of a particle which gets trapped by the cavity. It is compared to the trajectory that the particle would follow under the influence of a merely adiabatic potential. The simulation was initially written by S. Nimmrichter [34]. It basically solves the coupled equations 2.9, 2.14 & 2.15 numerically.

Additionally, an energy diagram is presented in which the evolution of the particle's total energy as well as the shape of the adiabatic potential are plotted. The steep slope of the potential towards $r = 0$ represents the centrifugal barrier. It inhibits the particle to approach the center of the cavity field. If one followed the simulation for a longer time, the particle would end up circling around the cavity center at a distance which is merely determined by its initial angular momentum.

2.2 Effects for extended particles

So far we have discussed the dynamics of polarizable point-like particles coupling to the Gaussian part of the cavity mode function. In our real-world experiment we observe molecular droplets ranging from a few 10 nm up to over 10 μm . When extended particles interact with the standing wave inside the resonator a point-like treatment is no longer valid. A more precise discussion of the various effects, which appear in this case, can be found in the PhD thesis of S. Nimmrichter [34].

In this particle size regime, the contribution of higher-order multipole components to the scattering properties of the particles cannot be neglected. Mie theory provides a solution, since it can describe the cavity field in the presence of a large nanoparticle.

This allows one to deduce a size dependent time averaged force acting on the center of mass of a particle interacting with the standing wave. In contrast to a point-like particle, for extended objects the force does not grow with the sphere volume any longer (for further information see reference [35]). In other words, an extended particle averages over the standing wave resulting in an effective coupling $U_{eff} < U_0$. Furthermore, for particles with diameters³ larger than $\lambda_{eff}/2$ one can observe that the force flips sign. In this case, the particle becomes an *effective low-field seeker* as its center of mass gets effectively attracted by the nodes of the standing wave field.

Schematically this effect is illustrated in figure 2.5: In panel a), the particle size is below $\lambda_{eff}/2$. Therefore, as most of its constituents are attracted by the anti-node of the field, it acts as a normal high-field seeker. In contrast to that, the size of the particle

³One additionally has to take into account that large particles strongly couple to the resonator field and consequently may change the structure of the standing wave locally. This results in an altered periodicity, which is denoted by λ_{eff} .

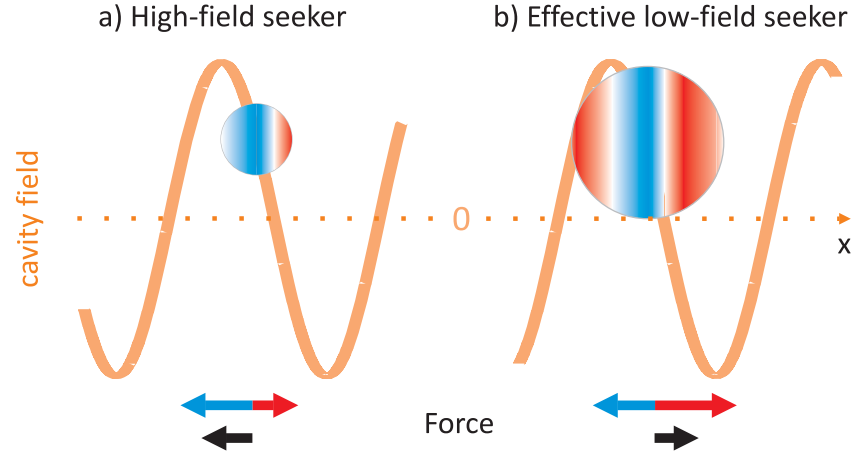


Figure 2.5: Comparison of the forces acting on two different sized particles which couple to a standing wave field. Both are placed in between a node and an anti-node of the field. The blue coloured areas represent parts which are attracted in direction of the anti-node and the red coloured ones in direction of the node. The resulting net force is depicted below.

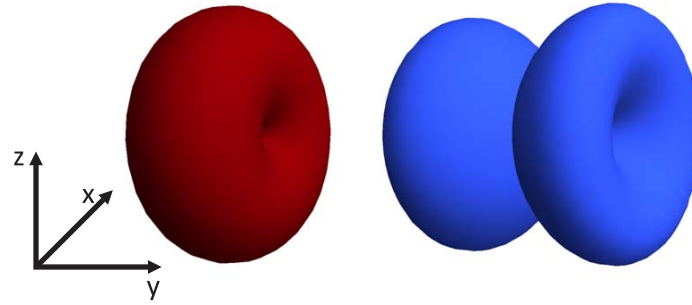


Figure 2.6: Radiation patterns for the dipole (left, red) and quadrupole (right, blue) components of the scattered light in a pump field with polarisation along y . The lengths of the vectors represent the intensity of the light scattered in the corresponding directions. The dipole pattern is strongly suppressed in y direction. The quadrupole component of the scattered light vanishes in the x - z plane that intersects the scattering center. Both components will be measured separately by two different detectors, as it will be discussed in section 3.4.3.

2.2 Effects for extended particles

in b) exceeds $\lambda_{eff}/2$ and different parts of the sphere experience opposite forces. This results in a net force pointing towards the low-field region and thus in an effective low-field seeking behaviour.

The scattered field of a particle can be expanded in a series of multi-pole moments. With growing particle size the relevance of higher-order components increases. The field of a point particle is well described by the dipole component (*Rayleigh scattering*). For bigger particles, which we also observe in our experiments, the quadrupole component and even higher order moments contribute to the scattering field (*Mie scattering*). These moments differ in the following ways:

In a linearly polarised field they exhibit different radiation patterns, which are depicted for the dipole and quadrupole components in figure 2.6 respectively. Therefore, these different moments can be distinguished spatially and detected as it will be discussed in section 3.4.3.

Additionally, the dipole and quadrupole moments differ in their periodicity along the standing wave. The dipole scattering power exhibits a maximum when the particle is placed in an anti-node of the field, whereas the power of the quadrupole component is maximal in a node of the field.

In this way the scattered light reveals information about the position of a particle within the standing wave. We will utilize this tool for characterising the high-field and effective low-field seeking behaviour for smaller and bigger particles in section 4.4 respectively.

3 Experimental Set-up

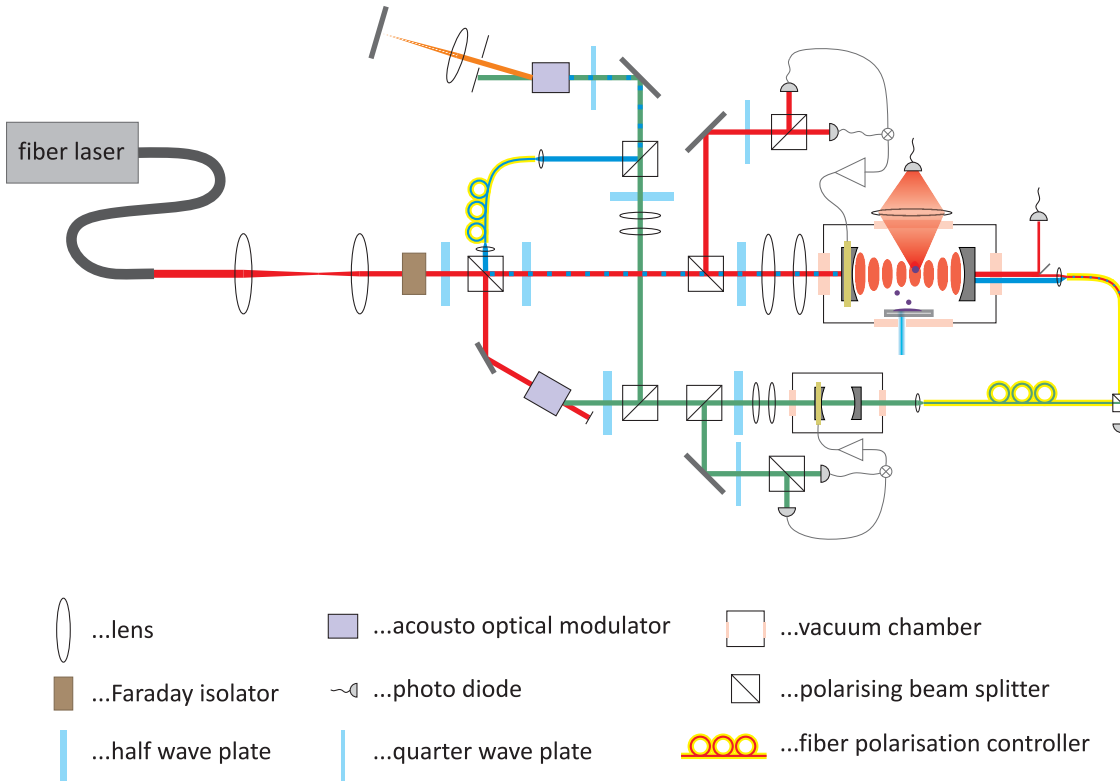


Figure 3.1: Schematic overview of the whole experimental set-up. Details will be explained in the following sections.

In this chapter we will describe the experimental set-up that was built up in our lab to show first manipulation effects on molecular droplets using intense light fields in a resonator. It is based on a scheme discussed in reference [36]. Since the set-up was adapted and optimized several times during the thesis, we will present the version used for the experiments in section 4.

The set-up can be split into three main components: An optical part for preparing the laser beam in order to pump and stabilise the cavity. A vacuum system in which the

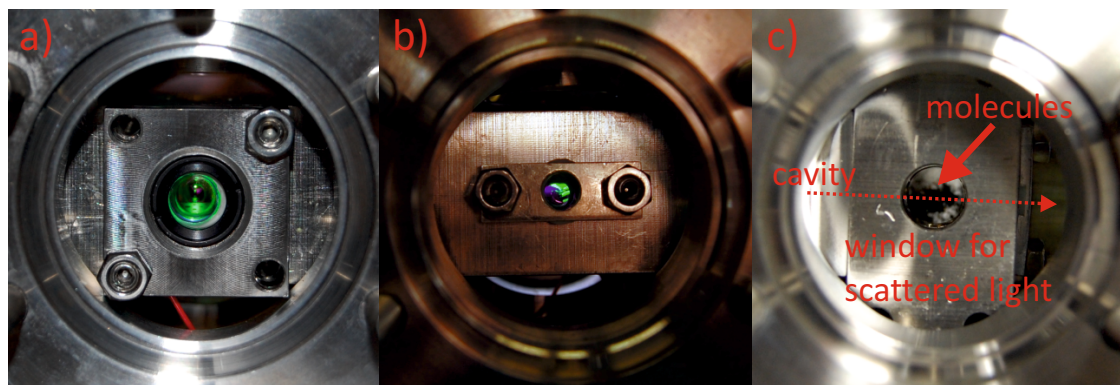


Figure 3.2: Pictures from the front side (a), back side (b) and from top of the cavity (c).

cavity is housed and the nano-droplets are produced, such that they can interact with the cavity fields. And finally a part for detection of various signals in order to characterise the dynamics of both the particles and the cavity. Figure 3.1 shows a schematic picture of the whole set-up. In the following sections we will explain and characterise its different parts in detail.

3.1 Cavity design

The cavity consists of two specially coated highly reflecting mirrors (Transmission < 2 ppm) from *ATFilms* with a diameter of 7.75 mm. Their radius of curvature equals 25 mm. As shown in figure 3.2 (a), an SM-05 retainer-ring presses a rubber ring, a piezo electric transducer ringer and the first cavity mirror against the cavity block, which is fabricated out of Invar. This is a nickel iron alloy that is notable for its low thermal expansion coefficient (≈ 1.2 ppm K $^{-1}$ at room temperature). The piezo transducer from *Piezomechanik GmbH* shows a high resonance frequency of above 300 kHz and a stiffness of 1800 N μm^{-1} . A mount on the back-side (fig. 3.2 b) presses the second cavity mirror against the cavity block via a Teflon ring. The length of the cavity equals about 25 mm, such that it is close to confocality. The deviation from the confocal configuration results in a frequency shift between the fundamental and the TEM $_{11}$ mode of about 30 MHz. Due to thermal effects the exact value depends on the intra-cavity intensity, as discussed in section 4.7. The cavity exhibits a linewidth of $\kappa \approx 2\pi \times 105$ kHz which corresponds to a finesse of $F = 2.9 \times 10^4$. Its waist equals to 79(1) μm . The whole block is housed in a vacuum chamber at a pressure below 1×10^{-7} mbar.

3.2 Pumping and stabilising the cavity

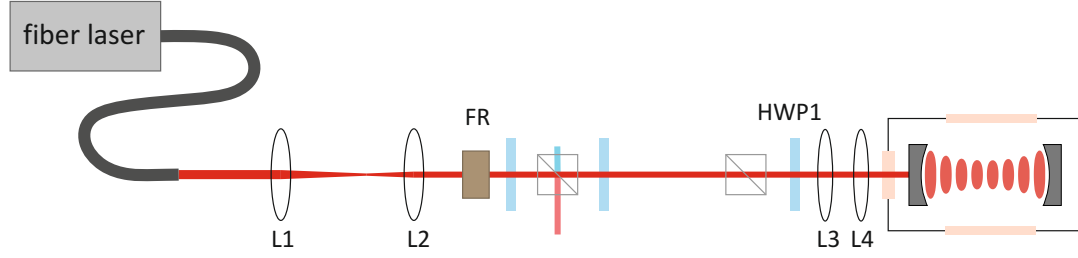


Figure 3.3: Set-up for pumping the fundamental cavity mode. The spot size of the fiber laser is reduced in a Kepler telescope (L1 & L2). A Faraday rotator (FR) secures the laser from harmful back-reflections. The polarisation of the pump light can be controlled via a half-wave-plate (HWP1). For optimising the mode-matching, the lenses L3 & L4 control size and focus of the pump beam.

3.2.1 Pumping the fundamental mode

The coherent light for the experiment is provided by the *ELR-10-1560-LP-SF* continuous-wave fiber laser from *IPG Photonics*. It has a wavelength of 1560 nm, a maximum output power of 10 W and a short time (50 ms) FWHM line-width of 20 kHz. It emits a linear polarised TEM_{00} mode with a $1/e^2$ diameter of 3.6 mm. Since this spot-size is too large for the following optical components, it is first reduced below 1 mm in a Kepler telescope (L1 & L2).

A Faraday isolator *IO-5-1550-HP* from *Thorlabs* is put into the beam path in order to protect the laser from harmful back-reflections.

To pump the fundamental (TEM_{00}) mode of the cavity effectively, the shape, the position, the incident angle and the focus of the pump beam have to be matched to it. First, the size and the focus of the incident beam waist have to be altered. For this purpose, we use two lenses (L3 & L4), which are mounted onto a rail, such that they can be aligned without changing the beam path.

For optimising the position and incident angle of the pump beam we use two mirrors mounted on two translation stages respectively. The polarisation of the pump field can be rotated by a half-wave-plate (HWP1).

In this set-up, mode-matching of up to 85 % is achieved. During the measurements, intra-cavity intensities of up to 25 kW are reached.

3 Experimental Set-up

3.2.2 Pumping a higher-order TEM mode

In some experiments we also weakly pump the HG-TEM₁₁ mode. Its transversal structure (figure 3.4 b) enables us to obtain insight into the path the particles follow through the resonator. We are able to measure the phase shift which is imposed when it crosses one of the lobes of the mode.

Figure 3.4 (a) shows the parts of the optical set-up which are needed to pump this higher order mode. Since the TEM₁₁ mode is shifted from the fundamental mode by +30 MHz, we also have to shift the frequency of the pump light. For this purpose, we use two acousto optical modulators (AOM1 & AOM2) *AMF-40-5-1560* from *Brimrose Corporation*. One for shifting the frequency by −60 MHz and the other in a double-pass configuration [37] by twice +45 MHz. This results in a total shift of +30 MHz. A portion of the light shifted by −60 MHz will be used as a local oscillator.

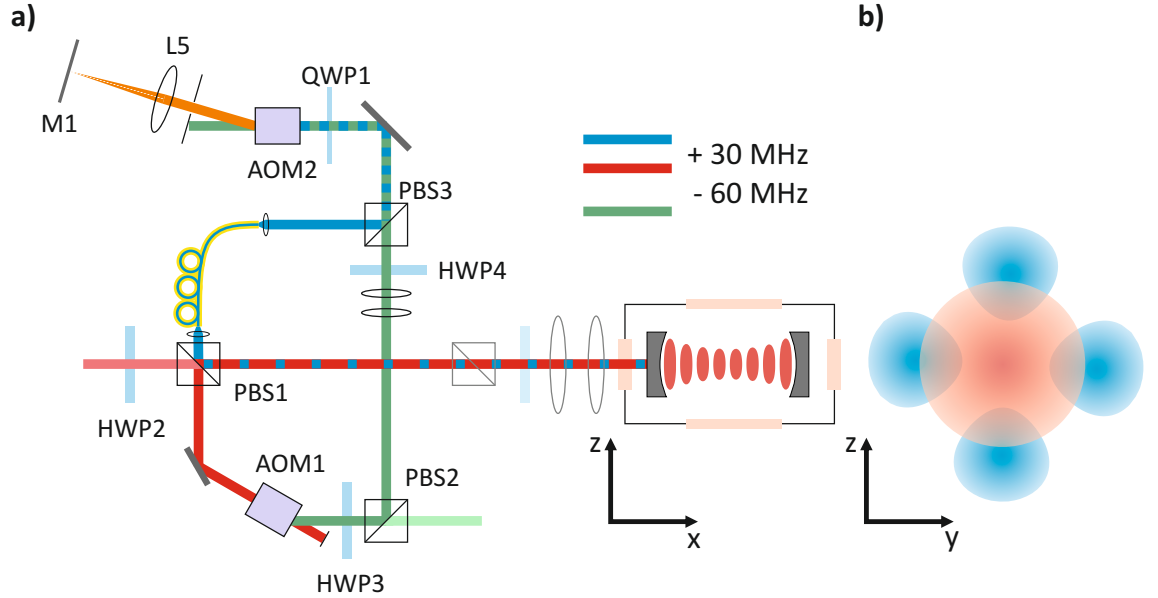


Figure 3.4: Set-up for pumping the TEM₁₁ cavity mode (a) which is depicted as blue in (b) together with the fundamental mode (red). The frequency of the pump light is in total shifted by +30 MHz via two acousto optical modulators (AOM1 & 2).

In principle, an acousto optical modulator operates in the following way: A radio-frequency (RF) signal is fed into a strain transducer which is in contact with the acousto optical crystal. The RF modulation causes a travelling density wave to form inside the crystal and therefore the refractive index of the medium is modulated. Consequently, the crystal acts like a thick diffraction grating which moves away from the transducer

3.2 Pumping and stabilising the cavity

at the speed of sound. For light entering at the Bragg angle, an inelastic scattering process in the crystal takes place which converts phonon into photon momentum and a frequency shifted beam is diffracted away from the direct and unaffected component.

We use a polarising beam splitter (PBS1) to extract some of the laser light. The splitting ratio can be controlled via a half-wave plate (HWP2). This light then passes through the AOM1, which is driven by 60 MHz. We use the first order diffracted beam, that is shifted by -60 MHz. The zeroth order beam is blocked. Again we use a half-wave plate and a polarising beam splitter (HWP3 & PBS2) for splitting the light. In this way, some of the light will be used as a local oscillator for a heterodyne-like detection scheme for the phases of both modes, as described in section 3.4.

In order to fit the spot size to the active aperture of AOM2, the beam diameter is reduced in a Kepler telescope (L5 & L6). Another half-wave plate turns back the polarisation to horizontal, such that the beam passes through PBS3.

After passing through AOM2 a pinhole blocks the unshifted beam. The diffracted beam passes through a lens (L7), which is positioned at a distance from the AOM that equals to its focal length. As the modulation frequency of the AOM is altered, the angle of diffraction is changed accordingly. But in this special configuration, when a lens is positioned at a distance f from the AOM, the rays emanate from its focal point and a variation of the modulation frequency only causes a parallel shift of them beam.

A mirror M1 can be aligned orthogonally to the diffracted beam such that it is always back-reflected through the AOM, where it is subjected to a second frequency shift and is overlapped with the incident beam. Therefore, the AOM can be operated within a frequency range of the order of a few MHz around its modulation center frequency without causing a beam displacement. This allows us to tune the frequency of the beam for pumping the TEM_{11} mode.

AOM2 is operated at $40 - 50$ MHz such that after the double-pass the beam is frequency-shifted by $80 - 100$ MHz. Consequently, the TEM_{11} pump beam is $20 - 40$ MHz apart from the TEM_{00} pump beam. The modulator is driven by the *ADF-4360-9 evaluation board* synthesizer from *Analog Devices*, which is additionally amplified. The frequency shift can be easily tuned in order to keep the TEM_{11} mode resonant during the measurements.

If one chooses the distance between mirror M1 and lens L7 to be equal to the focal length f , the back-reflected beam is collimated.

Since the back-reflected beam passes through the quarter-wave plate (QWP1) twice, in the end its polarisation is vertical and it can be separated from the incident beam by PBS2 before it is coupled into an optical fiber. A fiber polarisation controller serves

3 Experimental Set-up

for maintaining the vertical polarisation. Finally, the light is coupled out of the fiber and is overlapped with the cavity pump beam at PBS1. By tilting the output-coupler slightly and adjusting the focus, the mode-matching ($\sim 1\%$) for the TEM_{11} mode can be optimised.

3.2.3 Stabilisation of the cavity

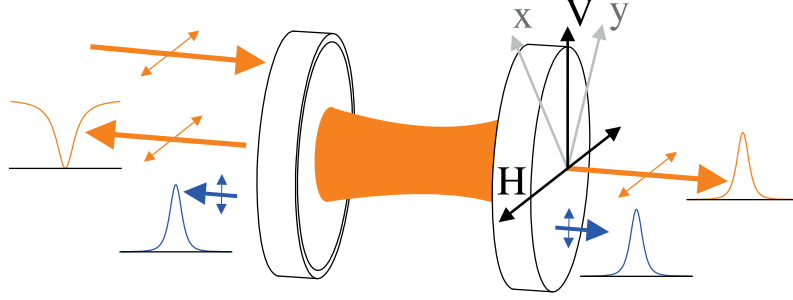


Figure 3.5: Polarisation scheme for stabilising the cavity based on weak mirror birefringence (WMB). In addition to the beam, which is back-reflected from the first cavity mirror, some light is emitted collinearly back with orthogonal polarisation. An error signal for locking the cavity can be obtained as described in the text. Figure taken from [38].

Our laser shows a short term (50 ms) linewidth of 20 kHz and thermal drifts on a time-scale of seconds. For this reason we need to lock the length of our cavity onto the laser frequency using a Weak Mirror Birefringence locking scheme (WMB) [38]. It is based on the intrinsic birefringence of the cavity mirrors, which can be caused by stress in the mirror substrate or coating and which may also be tuned by applying external mechanical stress. There exist a fast (\mathbf{x}) and a slow (\mathbf{y}) axis of birefringence. As shown in figure 3.5, when a linear laser field enters the cavity on resonance, the back-reflected intensity reaches a minimum for the same polarisation. Due to the birefringence, the intracavity field is slightly rotated such that some light is emitted collinearly back into the incident beam with an orthogonal polarisation. By decomposing both polarisations in the basis of \mathbf{x} and \mathbf{y} and subtracting their intensities $|E_x|^2$ and $|E_y|^2$, due to the phase difference γ between them, one obtains a dispersive error signal S . To first order in γ it can be written as

$$S(\delta) = |E_y|^2 - |E_x|^2 \approx \gamma E_0^2 \frac{R(1-R)^2 \sin(\delta)}{(1+R^2-2R\cos(\delta))^2}. \quad (3.1)$$

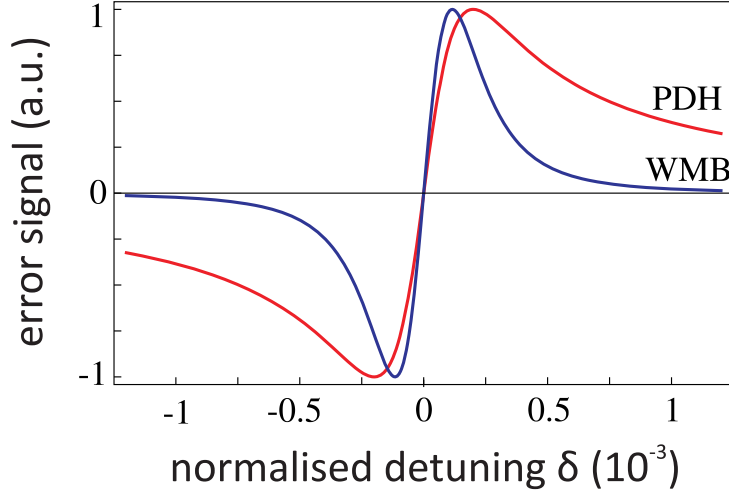


Figure 3.6: Calculated error-signals as a function of the cavity detuning: WMB compared to Pound-Drever-Hall. Curves taken from [38].

In this formula, R denotes the reflectivity of the mirrors and δ the normalised detuning, which is the ratio of the laser-cavity detuning and the cavity free spectral range.

The shape of the error signal is shown in figure 3.6. It is compared with the corresponding error signal for a Pound-Drever-Hall (PDH) locking scheme [39], which is commonly used in other cavity experiments. The WMB locking curve turns out to be narrower than the PDH line and in contrast to the PDH method, the WMB scheme does not need any modulations of the optical elements.

Experimentally we realise this locking scheme in the following way (fig. 3.7): A polarising beam splitter (PBS4) extracts the vertically polarised component of the back-reflected beam. Due to imperfections of the PBS, also 1 % of the horizontally polarised component of the backreflected beam is reflected. Now, both polarisation components are mixed by a quarter-wave plate QWP2. They are guided to PBS5, where they are again separated and detected by two photodiodes D1 & D2, respectively. Finally, their photocurrents are subtracted from each other. QWP2 is adjusted such that for the off-resonant cavity the error signal is zero. Close to resonance light enters the cavity and therefore an additional polarisation component is added to the back-reflected beam. This results in a non-zero error signal. By scanning over the resonance, the calculated error signal (fig. 3.6) can be reproduced.

In this set-up, the WMB locking scheme works best for stabilising a cavity on or close to its resonance. Since we are also using a second cavity for filtering purposes (section 3.4), which operates best at zero detuning, it can be applied there. For the cooling cav-

3 Experimental Set-up

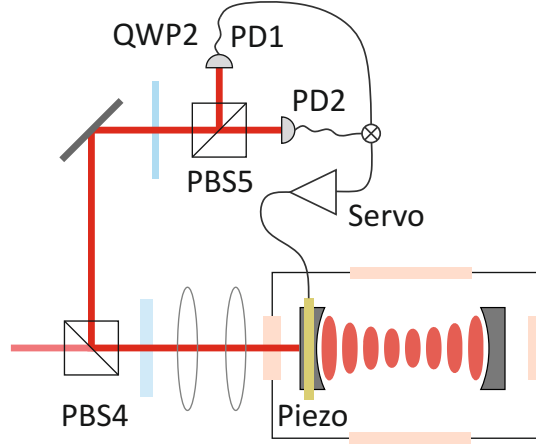


Figure 3.7: Set-up for locking the cavity in the WMB scheme. The polarising beam-splitter PBS4 extracts a mixture of light leaking out of the cavity and a small portion of the beam which is directly reflected backwards from the first cavity mirror. Their polarisations are mixed by a quarter wave plate QWP2, split up by PBS5 and detected by the photo-diodes PD1 & PD2 respectively. An error signal can be obtained by subtracting their photo-currents. It is fed into a locking servo, which drives the piezo. The shape of the error signal is plotted in figure 3.6.

ity, which needs to be detuned by $\Delta = -\kappa$ the transmitted intensity provides an error signal, which is detected by a photo-detector behind the cavity. This locking mechanism is also known as fringe-locking [40]. Keeping the transmitted power at half its value with respect to resonance corresponds to a cavity detuning of one linewidth.

Finally, the error signal is fed into a locking servo, which drives the piezo transducer. The frequency at which the feedback loop exhibits a gain equal to unity values about 30 kHz.

3.3 Particle source

In our cavity cooling experiments we used fluorinated C_{60} and tetraphenylporphyrin with fluorinated side chains¹. The latter have been synthesized in Basel in the group of Prof. M. Mayor for application in molecule interferometry [10, 41]: They exhibit a high volatility and thermal stability. To launch them into the cavity, we utilize a laser evaporation technique, which was used in our group previously for ejecting single molecules of phthalocyanine in a far-field interferometer [42].

¹TPPF_{20-x+17x} with $x_{max} = 11$

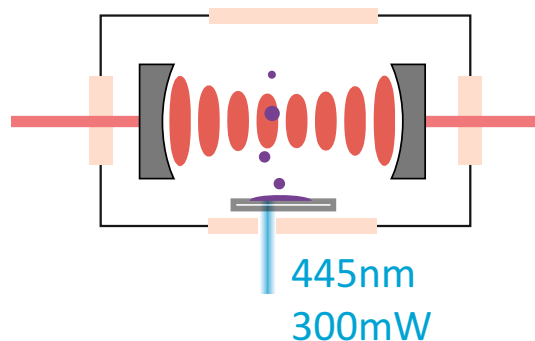


Figure 3.8: Set-up for launching molecular nanodroplets through the cavity. The molecular powder is placed on a quartz plate. It is heated locally from the back-side by a focused 300 mW laser beam at 445 nm. The molecules start melting, boiling and molecular nano- and micro-droplets are launched through the cavity. Their sizes and shape are depicted in figure 3.10.

The powder of molecules is placed on a small glass-window beneath the cavity within the vacuum chamber (see Fig. 3.8). A focused blue diode laser (cw, $\lambda = 445$ nm, $P \approx 300$ mW) heats them locally for 1.25 s and causes them to melt, boil and bubble. It turns out that during this process nano- and micro-droplets of a size between a few 10 nm up to over 10 μm are formed and ejected. Their forward velocity ranges from about 1 to 50 m s^{-1} .

In order to characterise their shape and size distribution in more detail we studied them under the transmission electron microscope² in the group of Prof. J. Meyer. Figure 3.9 shows such a typical droplet of about 300 nm in diameter, which exhibits an almost perfect spherical shape.

We succeeded in producing nano- and micro-droplets from TPPF₈₄ and the amino-acid Tryptophan³ by the same method. The results for Tryptophan are depicted in figure 3.10. They exhibit a large variety of sizes, whereas in most cases they emerge as spherical droplets. The structures of the molecules can be found in the supplements 6.1.

3.4 Detection of the cavity and particle dynamics

In order to understand and characterise the particles' motion through the cavity, we detect four different signals. All of them are recorded with a *Razor 1642 Express CompuScope* digitizer from *GaGe*. It features 16-bit resolution at a sampling rate of 200 MS s^{-1}

²Philips CM200 with an acceleration voltage of 200 kV.

³C₁₁H₁₂N₂O₂

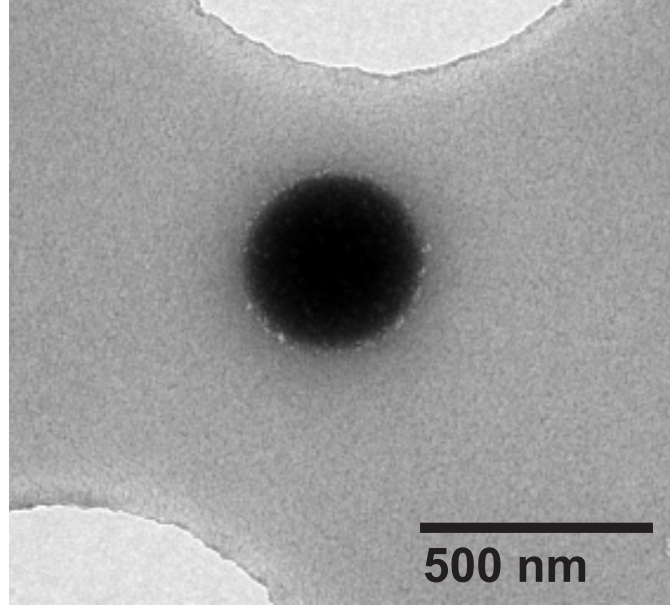


Figure 3.9: TEM-picture of a TPPF_{20-x+17x} droplet with a diameter of 330 nm.

with an input bandwidth of 125 MHz for 4 channels and is directly connected to the PCI-Express port of our Lab-PC. It is externally triggered, such that it starts collecting data for 1.25 s at full sampling rate when the evaporation laser is switched on. We additionally use an external 10 MHz oscillator clock in order to synchronise the digitizer, AOM1⁴ and the synthesizer, which is used for driving AOM2.

We detect the following signals:

3.4.1 Transmitted intensity through the fundamental cavity mode

In order to obtain some information about the intra-cavity intensity of the fundamental mode we detect the light that leaks out of the second cavity mirror in photo-diode D1. This signal however does not directly reveal the trajectory of the particle, since it reacts to the droplet position on a time-delayed scale. Additionally it is quite noisy due to the power and phase fluctuations in the laser-cavity system.

3.4.2 Phase and amplitude of TEM₀₀ & TEM₁₁ modes

The phase of the fundamental mode reveals information about the dielectric properties of the particles. The phase shift, which is caused by a droplet flying through the cavity

⁴AOM1 is driven by multiplying the oscillator clock by a factor of 6 and amplifying this signal.

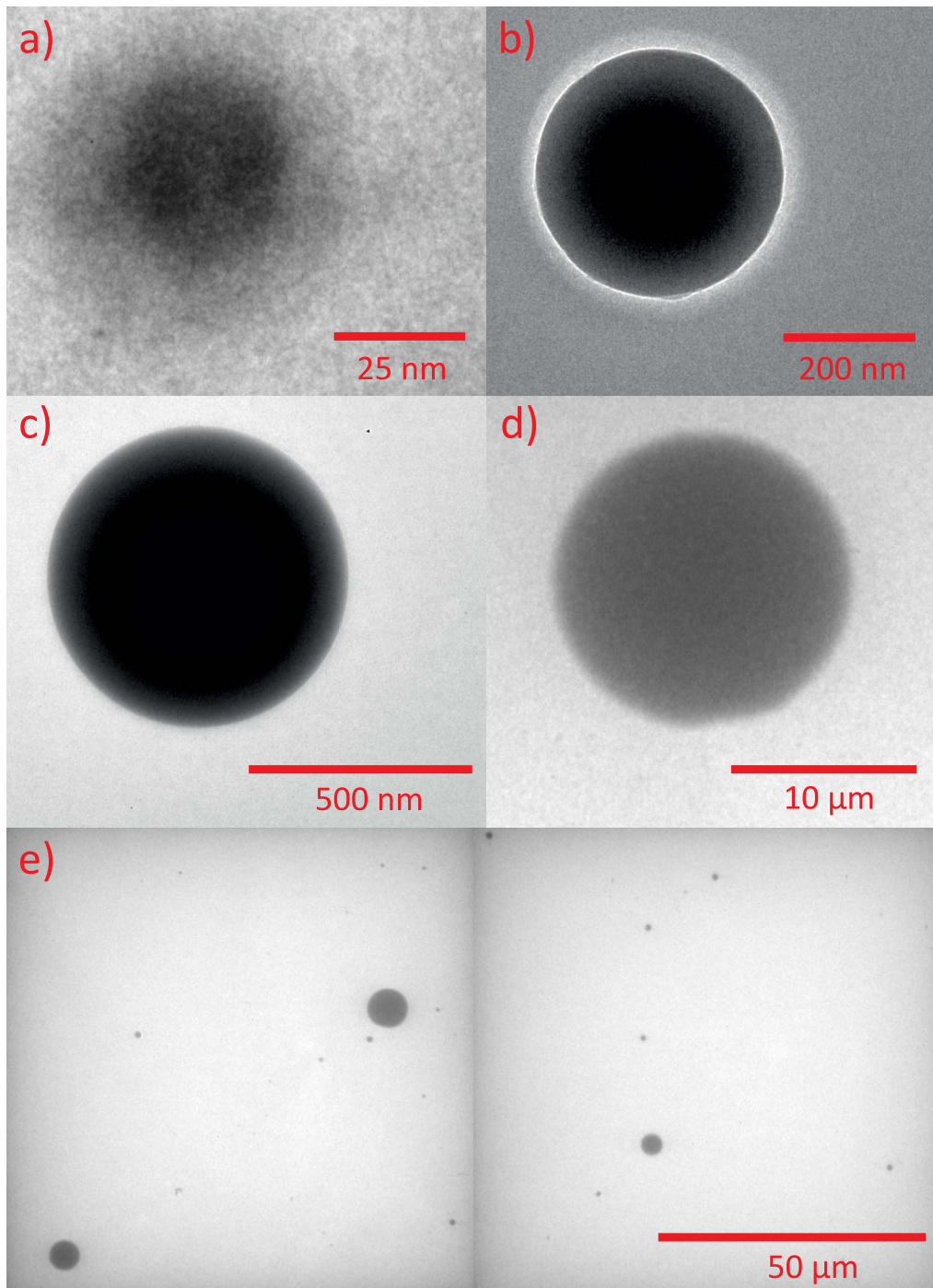


Figure 3.10: Pictures of Tryptophan droplets. Diameters: a) 30 nm, b) 380 nm, c) 670 nm and d) 15.8 μm. Picture e) shows the size distribution of the droplets on 2 typical fields on the TEM-grid. All images taken under the *Philips CM200* transmission electron microscope.

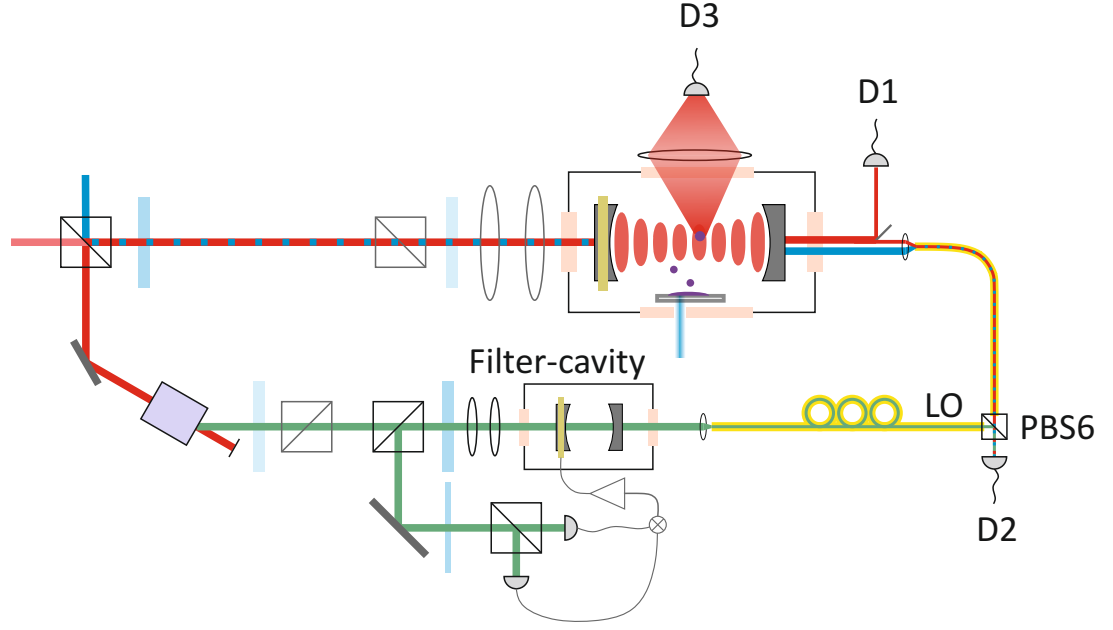


Figure 3.11: Schematic set-up for detecting the transmitted intensity through the fundamental cavity mode (D1), the phase of the fundamental and the TEM_{11} mode via a heterodyne-like detection (D2) and the light which the particles scatter out of the cavity modes (D3).

field, is proportional to the particle's polarisability α (see equ. 2.5) but also depends on its path through the mode (equ. 2.7). Thus, in order to determine α , one has to get further information about the trajectories taken by the particles. For this purpose we weakly pump the TEM_{11} mode and measure its phase and amplitude.

There are two options for determining phase and amplitude of a light field: Performing a homodyne- or a heterodyne measurement respectively. In a homodyning scheme, the signal beam interferes on the photo-diode with a beam that directly originates from the same laser source. Depending on their phase-difference, one obtains either the phase-quadrature, the amplitude-quadrature or a mixture of both. In order to select one of them, one needs to lock their phase-difference. This could e.g. be achieved by using a mirror that is mounted onto a piezo, which is driven by a locking servo that keeps the offset of the output signal at a certain value (e.g. at minimum in order to get the phase-quadrature).

Instead, we decided to perform a heterodyne-like measurement: We overlap the light behind the cavity, which is transmitted through one of both modes, with a local oscillator beam (LO) on PBS6 and detect it on D2. This results in an electronic beating signal.

Since the light from the two modes can be distinguished frequencywise, we are able to measure both quadratures for both TEM modes via a single digitiser-channel simultaneously. No phase-stabilisation is required and a full dynamic range can be achieved.

We just need an LO beam at a different frequency compared to our signal-beam. Its frequency is chosen to fit to the digitizer bandwidth, such that it enables us to record the full beating signals. As already mentioned in section 3.2.2, we therefore use the beam that is shifted by -60 MHz through AOM1. In order to eliminate other frequencies that may appear due to round-trips through the optical path and to get a sharp frequency peak in the spectrum, the LO beam is filtered via a filter-cavity, which is housed in a second vacuum chamber and stabilised using the WMB locking scheme.

Subsequently, the LO beam is coupled into an optical fiber and combined with the signal beam in a fiber coupler (*SCD1189-07* from *DiCon Fiberoptics Inc.*). The overlap of both TEM modes is coupled into the second input port of the fiber coupler. This results in a 60 MHz beating for the fundamental mode and a 90 MHz beating for the TEM₁₁ mode in the recorded signal. The amplitude of this beating can be maximized by adjusting the polarisation of the LO beam via a fiber polarisation controller accordingly. The beating is detected with a fast photo-detector D2 and collected by the digitiser. Out of this signal one can finally mathematically extract the phase and amplitude for both modes. The corresponding Matlab routine can be found in the supplements (6.2).

3.4.3 Scattered light

The scattered light gives us a real-time image of the particles' coupling to the fundamental mode as it is not time-delayed by the cavity dynamics. This signal shows both, the particles crossing the Gaussian beam profile as well as their motion over the standing wave. As already mentioned in section 2.2, big droplets cannot be treated as point-like particles any more. The bigger they are the more higher-order momenta contribute to the scattered light. Since for a linearly polarised cavity field the two lowest momenta can be distinguished from their spatial scattering pattern, it is interesting to place two photo-detectors (D3 & D4) along orthogonal directions (see fig. 3.12).

For a horizontally polarised pump field, the signal collected by D3 mainly consists of dipole parts, whereas the signal from D4 shows a high fraction of quadrupole parts of the scattered field. Especially in section 4.4, where we will discuss the effective low-field seeking behaviour of a big droplet, their difference will be of great interest.

The signals from D3 & D4 are used in a peak-finder routine to identify particles among the collected data. For this purpose it is advantageous that the scattered light only exhibits a non-zero signal when a particle transits the cavity mode.

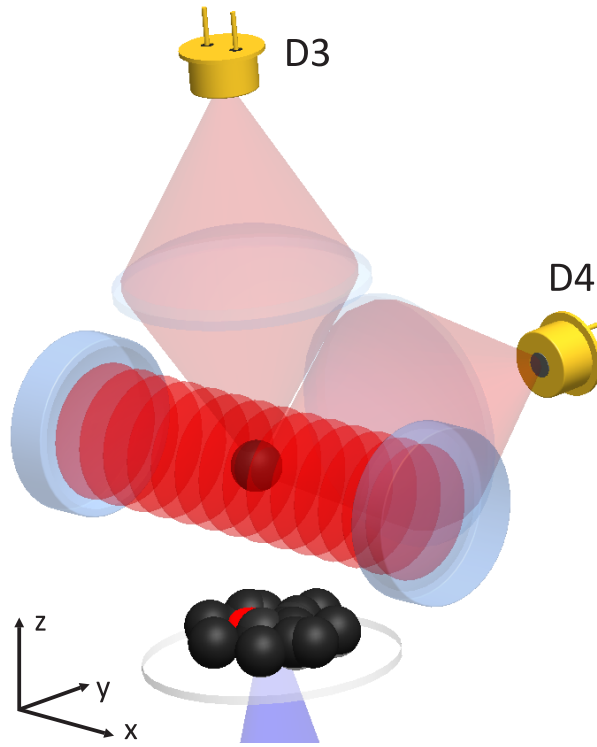


Figure 3.12: Detection scheme for the light that the particles scatter out of the cavity modes. Two photo-diodes D3 & D4 are positioned orthogonally in order to detect different parts of the scattered light. Their scattering patterns can be found in figure 2.6. The light detected by D3 is dominated by the dipole component, whereas the signal in D4 mainly consists of the quadrupole moment.

4 Results

Now, we want to present first experimental results that have been achieved with this set-up. Most of the measurements have been carried out during August 2012. We observe different kinds of cavity-particle interactions, which we will discuss in this chapter:

First, there are particles, which are basically unaffected by the optical potential since their kinetic energies are too high. It is however interesting to look at one of them in order to show how the cavity provides a way for detecting and characterising such particles. Furthermore, their trajectories can be estimated roughly from the various recorded signals and reconstructed in a simulation.

Since we also expect to observe effects in the direction of the cavity, we will then discuss a particle that is weakly trapped in the standing wave and exhibits phase-shift induced modulations of the intra-cavity intensity. Unfortunately it does not fulfil the conditions, which are necessary for cooling along the standing wave direction.

The next kind of particle that we want to present, is one that is strongly affected by the cavity dynamics. While it passes through the resonator, it gradually turns on the intra-cavity intensity. From the measured signals we can conclude that the droplet transits the resonator far off center and then returns through the cavity mode for a second time. As we will discuss, such an effect can not be explained by the cylindrical symmetric forces in a conservative steady state cavity potential.

As already discussed in section 2, for particles that reach a size of the order of $\lambda_{eff}/2$ we will observe an effective low-field seeking behaviour. In order to demonstrate this effect we will compare the scattering curves for a small and a bigger particle which are both trapped in the standing wave.

Furthermore, in these experiments we observe different kinds of dynamics that are not fully understood yet. Some of the droplets show an asymmetry in their scattered light that cannot be described by slowing effects. Therefore, we will present one of these curves and discuss possible reasons for such a behaviour. Other droplets exhibit a sudden change in their scattered light and seem to be deformed or even destroyed by the intense cavity field.

4 Results

Finally, we will discuss the limiting factors of this first experimental configuration. It turns out that thermally induced feedback counteracts the dynamics, which is necessary for cavity cooling. We will introduce this effect schematically and characterise it experimentally.

4.1 Detection of a droplet passing through the cavity mode

Figure 4.1 reveals the TEM_{00} phase shift, TEM_{00} intensity, TEM_{11} phase shift and the overall scattering intensity for a medium-sized particle which passes through the cavity mode without being affected by the field dynamics. In this measurement the cavity is pumped by approximately 2 W and detuned by $-\kappa$. The particle can be seen on all signals which allows us to characterise its properties as well as details about its dynamics.

First, we can determine its velocity along the x- and z-axis respectively: We divide the light I_S detected by photo-detector D3 (see fig. 3.12), through the transmitted intensity I_C detected on D1 and normalise it in the following way:

$$S_N \equiv \frac{I_S}{I_C} \cdot \max \left(\frac{I_S}{I_C} \right)^{-1}.$$

It is related to the mode function via

$$S_N \propto \sin^2(kx) e^{-2 \frac{x^2+y^2}{w^2}}.$$

The normalised scattering signal S_N reveals the coupling to the Gaussian envelope as well as to the standing wave. From the latter one we can extract the velocity in x-direction v_x , since the periodicity T_{osc} of the oscillation relates to the structure of the standing wave via $T_{osc} = \lambda/2v_x$.

In order to determine the forward velocity v_z of the droplet, one can fit the Gaussian envelope of S_N , extract the time T_{gauss} which the particle needs to pass through the cavity waist and consequently calculate its velocity via $v_z = w/T_{gauss}$. For the droplet shown in figure 4.1 we obtain $v_x = 0.78$ m/s and $v_z = 19.3$ m/s.

In the next step we can simulate the particle trajectory through the cavity in a Matlab simulation. The initial values for the particle dynamics are taken from the measured results. Figure 4.2 shows the outcomes for the simulation of the droplet dynamics presented in figure 4.1.

Comparing the signals, one can conclude that the phase shifts for the two modes as well as the coupling to the fundamental mode can be reconstructed quite well. Only

4.1 Detection of a droplet passing through the cavity mode

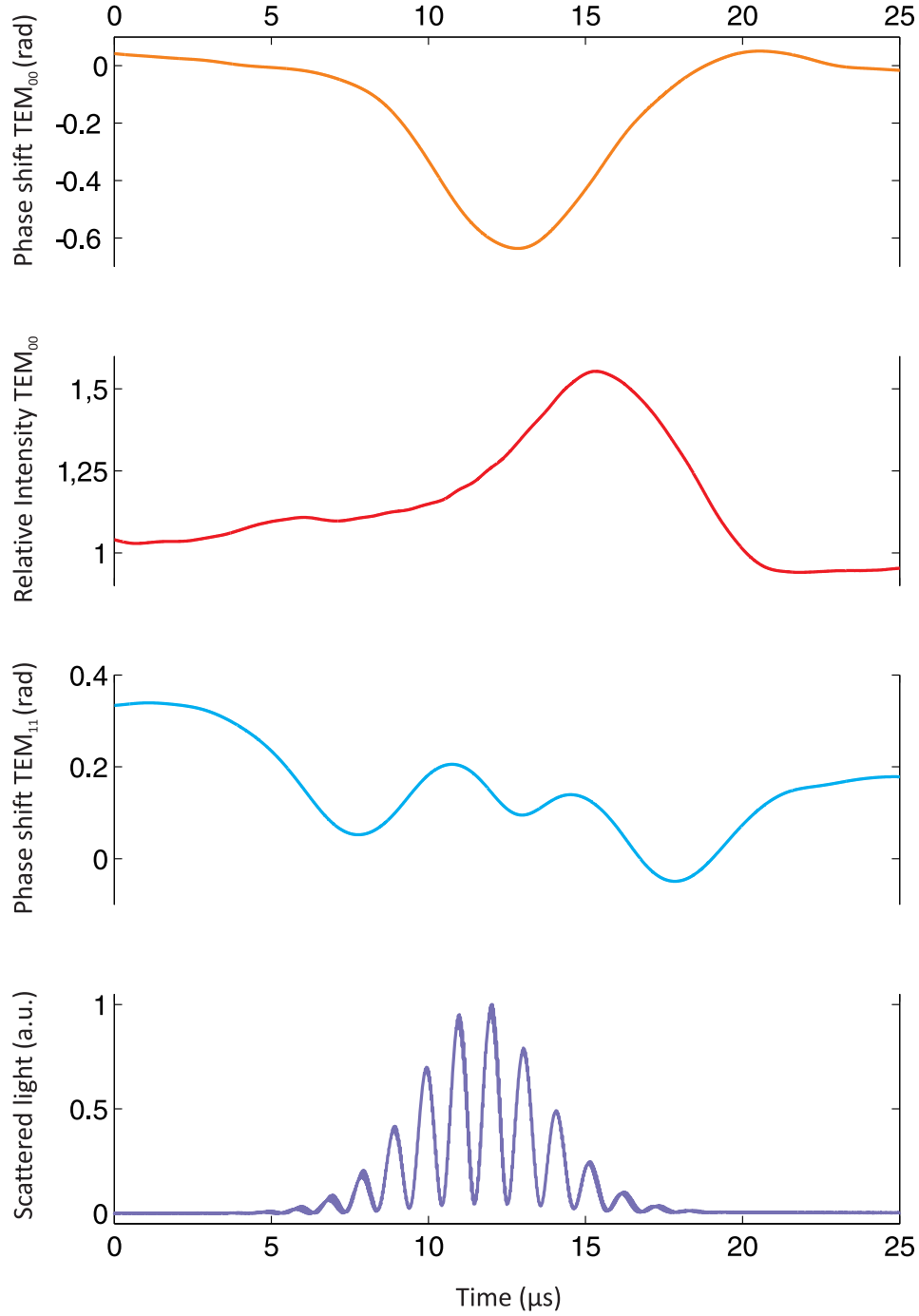


Figure 4.1: Detection of a $\text{TPPF}_{20-x+17x}$ droplet passing through the cavity. Starting at the top, one can see the phase of the fundamental mode, its intensity, the phase of the TEM_{11} mode and the normalised scattering behaviour. From the scattered light we can extract the particle velocities in x- and z-direction respectively. The phases of both modes provide a way to reconstruct the trajectory of the droplet via a computer simulation.

4 Results

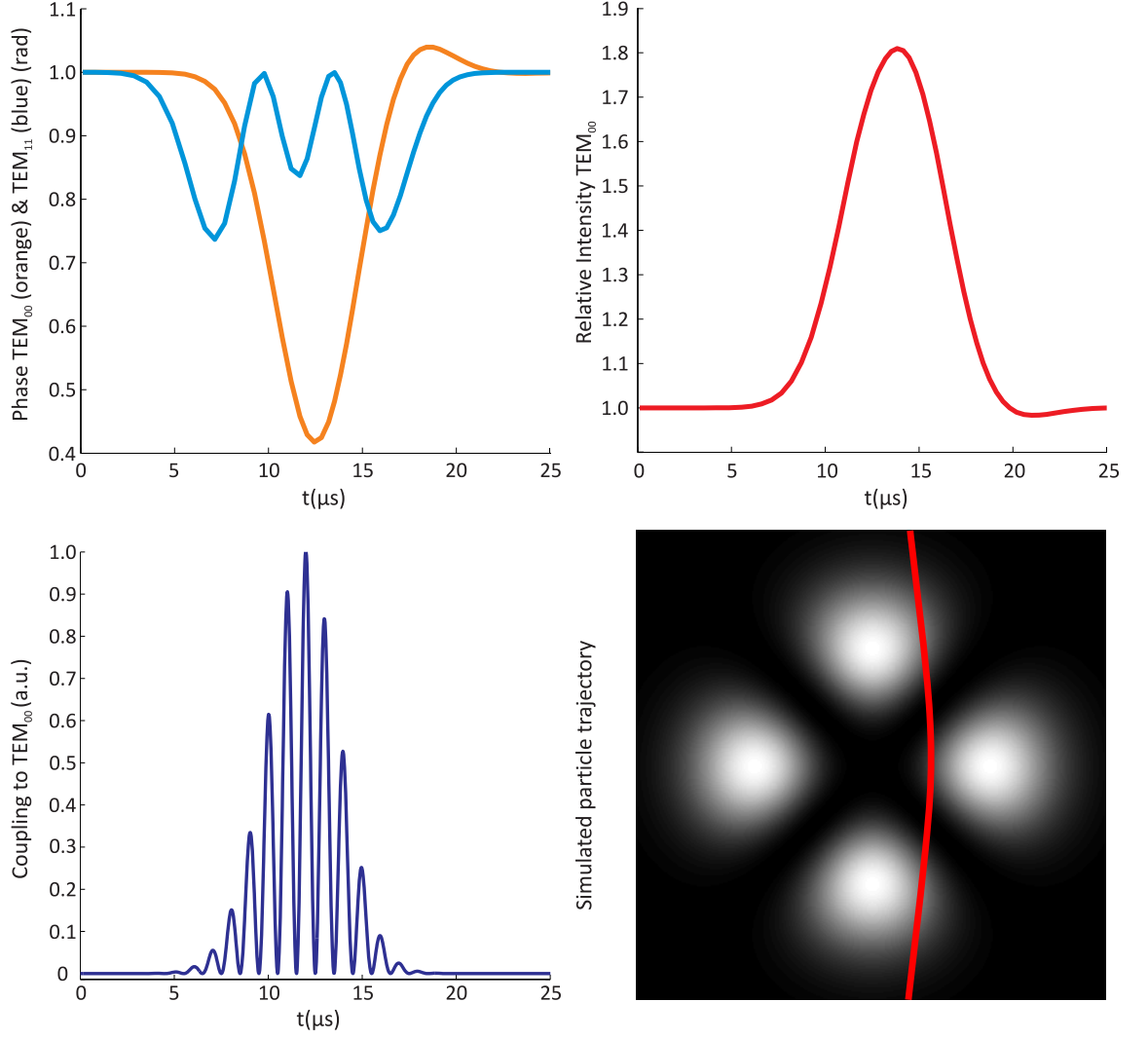


Figure 4.2: Simulation of the droplet shown in figure 4.1. The measured curves are reproduced and the particle's trajectory is plotted. The simulation slightly deviates from the experimental results due to a thermal feedback mechanism, which influences the real cavity dynamics (see section 4.7).

4.2 Channelling of a droplet through the standing wave

the simulated intensity does not fit very accurately to the measured curve. This can be explained by an additional damping factor that is caused by a thermal feedback effect in the mirror surface. It will be specified further in section 4.7.

From the simulation we obtain a coupling frequency of $U_0 = -1.5 \kappa$. Therefore, one can estimate the particle's polarisability α to be of the order of $4\pi\epsilon_0 \times 2 \times 10^{10} \text{ \AA}^3$. Assuming a polarizability of about $4\pi\epsilon_0 \times 280 \text{ \AA}^3$ per molecule¹ this yields about 7×10^7 molecules in the droplet and corresponds to a total mass of approximately $5 \times 10^{11} \text{ amu}$.

4.2 Channelling of a droplet through the standing wave

It is also interesting to look at effects that influence the particle motion along the cavity axis x . From the scattering behaviour of the droplet, which is shown in figure 4.3, we can conclude the following: When the particle approaches the middle of the fundamental mode it runs over the standing wave and thus shows a sinusoidal modulation of the scattered light with almost 100 % visibility (i). At some point (after about $7 \mu\text{s}$, approximately one cavity waist away from the center) the intra-cavity intensity is sufficiently high to weakly trap the particle in an anti-node of the standing wave. This results in a non-sinusoidal shape of the scattered light and a reduction of the fringe visibility. After about $13 \mu\text{s}$ the particle is already about one cavity waist past the center and thus the intensity does not suffice any longer to keep the particle trapped (iii).

The scattered light provides a way to reconstruct the trajectory of the droplet along the cavity axis in the following manner: We divide the normalised scattering signal S_N through a fit of its Gaussian envelope. Only the modulation, which is related to the coupling with the standing wave, remains. The position $x(t)$ can thus be extracted by

$$x(t) = \sqrt{\arcsin \left(S_N(t) \cdot e^{2\frac{v_z^2 t^2}{w^2}} \right)}. \quad (4.1)$$

Additionally one has to put in the following assumptions: Whenever the scattered light reaches a zero point it indicates that the particle crosses an anti-node of the standing wave. It thus continues flying in the same direction. In case of non-zero minima the droplet is trapped and therefore changes its direction of flight. Both at the zero-valued minima and at the maxima, S_N is least sensitive to the position of the droplet. Therefore, at these points the particle positions are extracted with least precision. This results in discontinuities of the reconstructed trajectory. This can however be smoothed

¹This value is taken from a calculation using Gaussian09 with the basis 6-31G.

4 Results

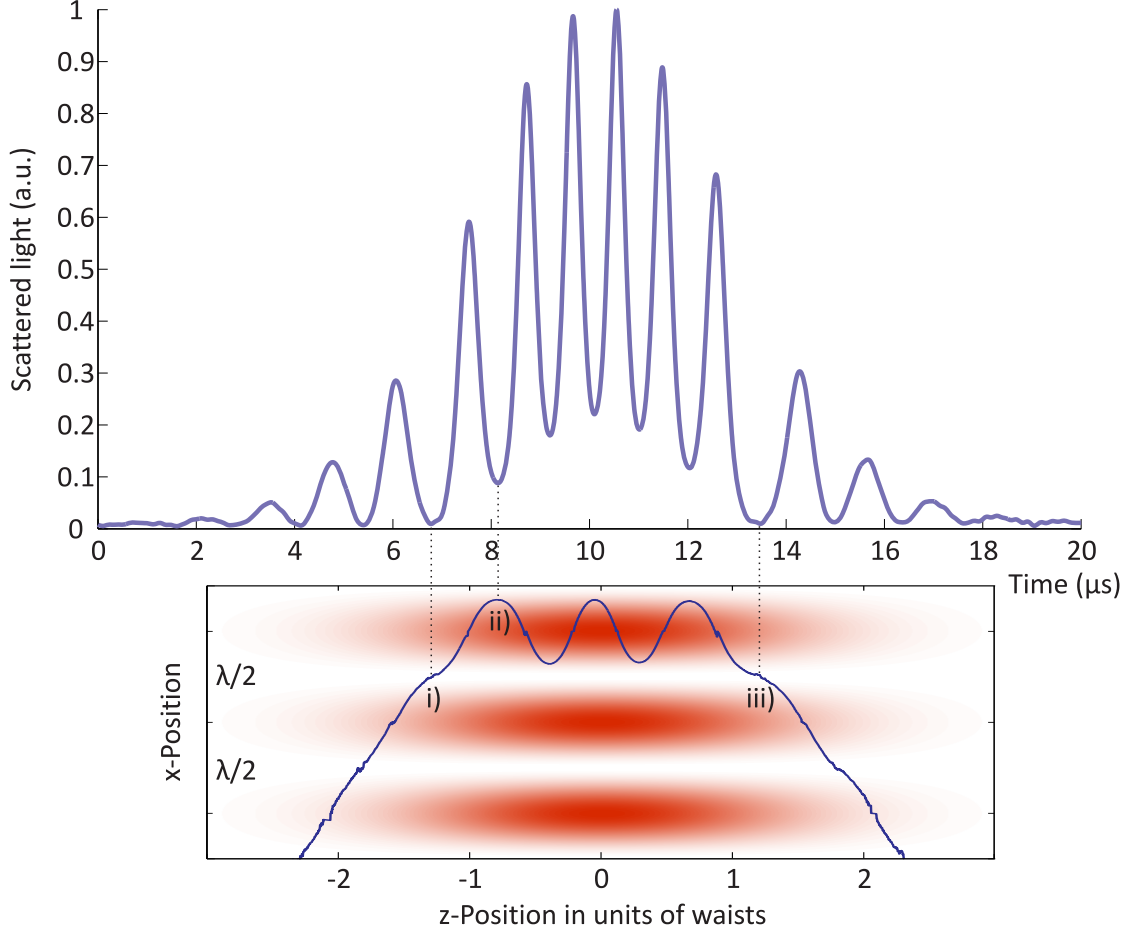


Figure 4.3: Scattering behaviour and reconstructed trajectory of a $\text{TPPF}_{20-x+17x}$ droplet that is channelled through the standing wave: (i), the sinusoidal modulation of the scattered light shows full visibility and thus the particle crosses a node of the field for the last time before the intensity is high enough to trap it in an anti-node (depicted by the red areas) of the field (ii), where it subsequently gets channelled. After five reflections the droplet is released again (iii). The methods for reconstructing the trajectory are described in the main text.

by linear regression. The corresponding Matlab code for these operations can be found in the supplements of the thesis (sec. 6.3).

The symmetry in the trapping and releasing process indicates that the particle hardly loses any of its kinetic energy. In order to test whether at least a small amount of cavity cooling along this direction took place, one has to examine the modulations on the cavity phase, on its intensity and on the scattered light, which are caused by the interaction of the droplet with the cavity field. They can be obtained by applying a band-pass filter (0.5 MHz - 2.5 MHz) to the respective signals. The results are shown in figure 4.4.

One can conclude that the velocity of the particle is too high for the chosen detuning or the particle scatters too much light out of the mode. As a result, the timing of the cavity dynamics does not fulfil the requirements, which are necessary for slowing the particle along either the z-direction or the cavity axis.

4.3 Cavity induced turning back of a droplet

In contrast to the droplet shown before, we now look at a particle that is strongly affected by the cavity dynamics. Again, we observe the phases of the TEM_{00} & TEM_{11} modes, the intensity transmitted through the TEM_{00} mode and the light, which is scattered by the particle. They are all plotted in figure 4.5.

From these signals we can conclude the following: The phase & intensity of the fundamental mode, as well as the scattering behaviour of the particle clearly indicate that the droplet approaches the center of the cavity twice, or in other words, that its radial coordinate reaches two local minima. As the fast modulation on the scattered light, which is caused by the particle's running over the cavity's standing wave, steadily continues over both peaks without changing its frequency and phase, one can conclude that during this measurement there is one single particle with a constant velocity along the cavity axis that couples to the cavity mode.

Looking at the particle dynamics, the following can be stated: When the droplet enters the cavity for the first time, it shifts the phase of the TEM_{00} mode towards resonance and thus permits more light to be coupled into the resonator. Additionally it strongly scatters light out of the cavity. This results in a drop of intensity. While the particle travels out of the resonator again, the intra-cavity intensity reaches its maximum. Due to thermal feedback of the cavity mirrors, which will be discussed at the end of this chapter, as well as due to fluctuations in the pump power, the interaction between the particle and the cavity dynamics is complex. For these reasons it is also very hard to simulate the dynamics of the particle and the cavity field in the same way as it has been

4 Results

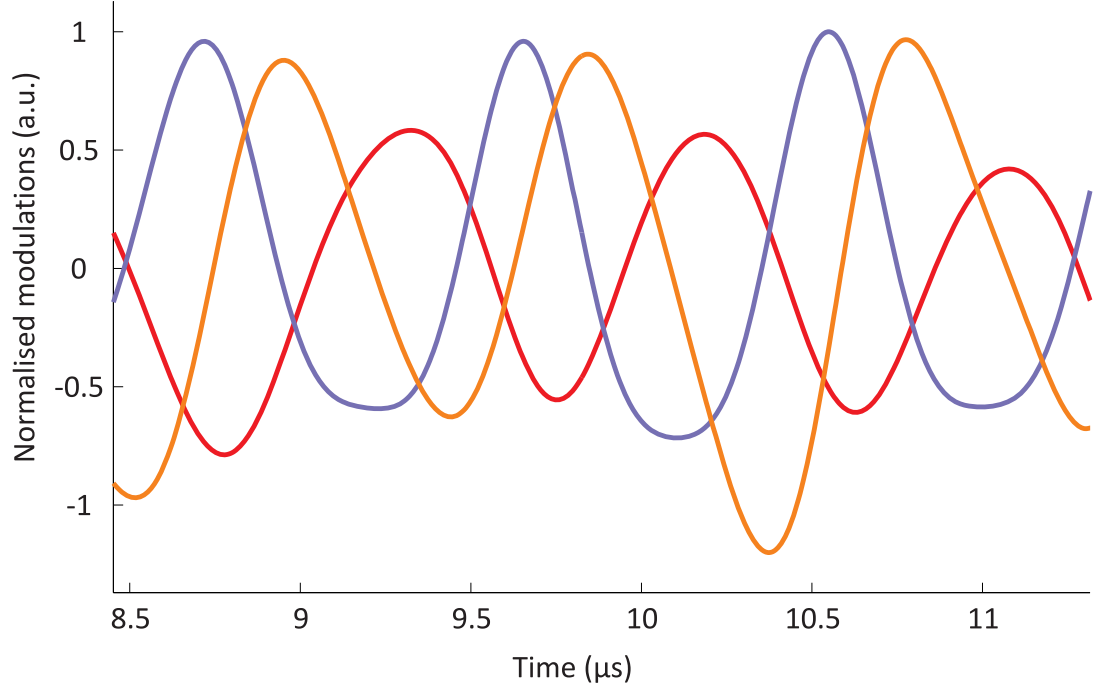


Figure 4.4: Droplet causing phase-shift induced modulations of the intensity inside the resonator while it is trapped in an anti-node of the standing wave. The modulations in the particles's normalised scattering (purple), in the phase-shift (orange) and in the intensity (red) are plotted against time. During each cycle the intensity reaches its maximum while the particle already approaches the next anti-node of the field. Therefore the conditions, which are necessary for cavity cooling along the cavity axis, are not fulfilled. This can either be a consequence of an insufficiently large detuning or of too much scattering out of the cavity field by the particle.

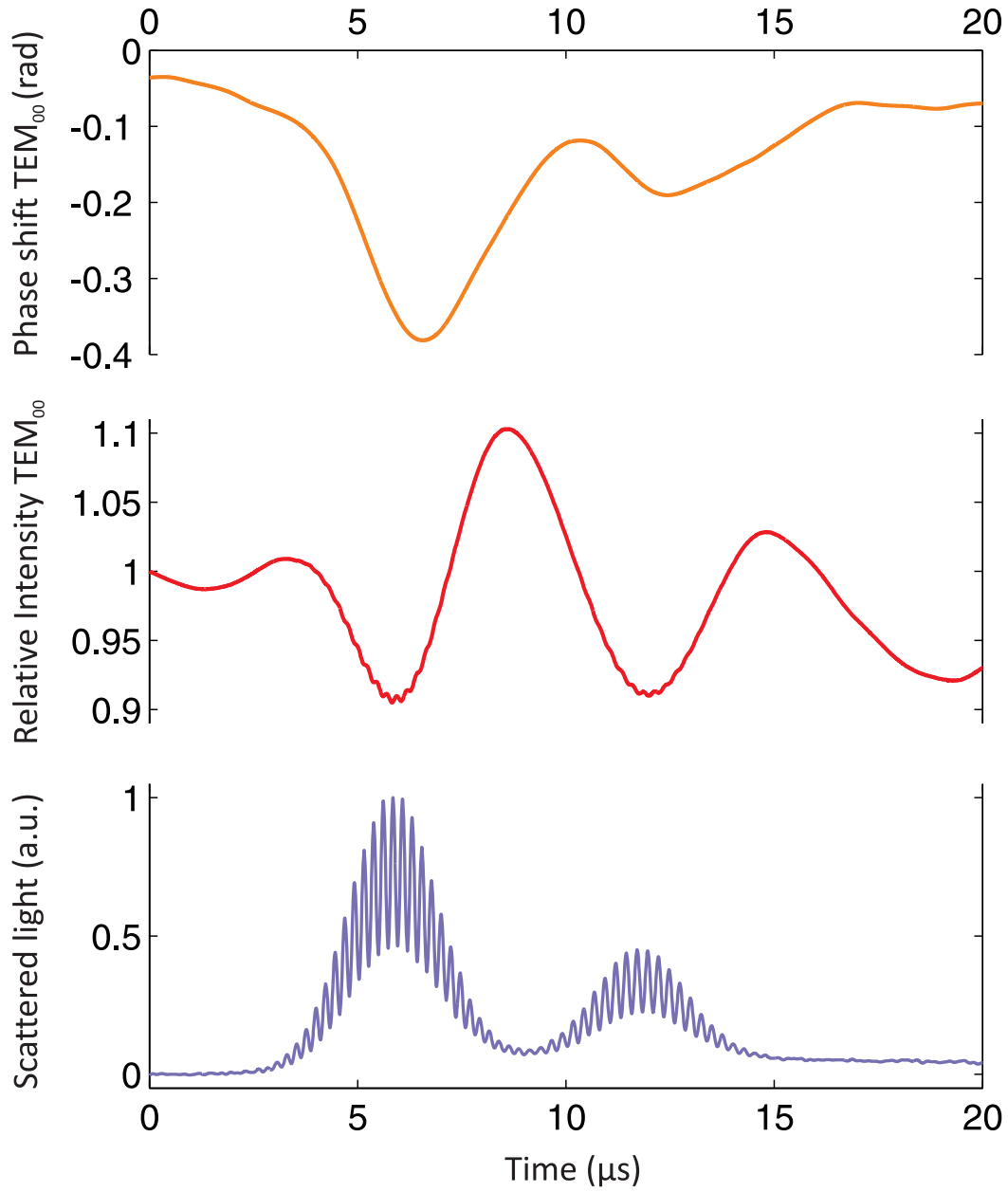


Figure 4.5: Measured signals for a $\text{TPPF}_{20-x+17x}$ droplet that passes through the cavity twice: The phase of the fundamental mode (orange), its intensity (red) and the normalised scattering behaviour (blue) are plotted against the transit time of the particle.

4 Results

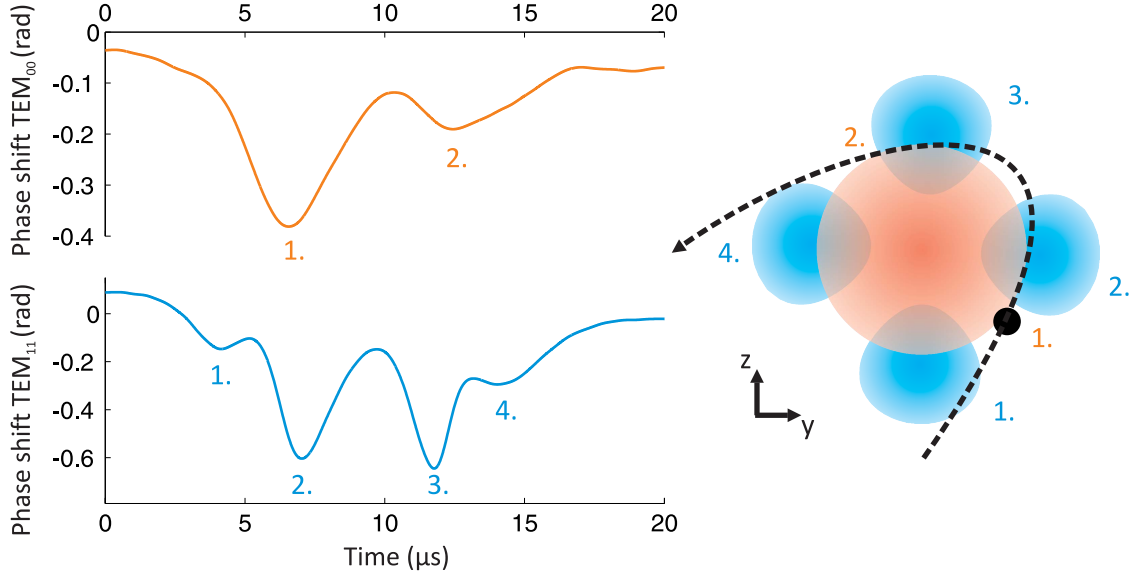


Figure 4.6: The trajectory (right) of the droplet through the cavity can be estimated roughly from the measured phase shifts of both the TEM_{00} and the TEM_{11} modes (left).

done in the previous case.

For this reason we can only estimate the particle trajectory through the resonator by interpreting the phase shifts it imprints onto both modes. Figure 4.6 shows a trajectory that fits to the measured signals most accurately. It seems that the particle transects the cavity far off center.

Such a trajectory can not be explained in case of a merely adiabatic potential. The reversion of the droplet is therefore a result of the non-conservative nature of the potential as well as supported by an asymmetry in the forces that act in y - and z -direction respectively. Such an asymmetry can for instance be caused by an elliptical beam waist or may be a consequence of Mie scattering for large particles with high indices of refraction [34].

4.4 Effective low-field seeking behaviour

We now look at a big droplet that interacts with the standing wave of the cavity. The scattered light, which is detected by the two photo-diodes D3 & D4, is plotted in figure 4.7. As discussed in section 2, the center of mass for particles with a diameter that effectively exceeds half the wavelength is subjected to a net force pointing towards a node of the standing wave. Consequently, it is effectively trapped in a low-field region

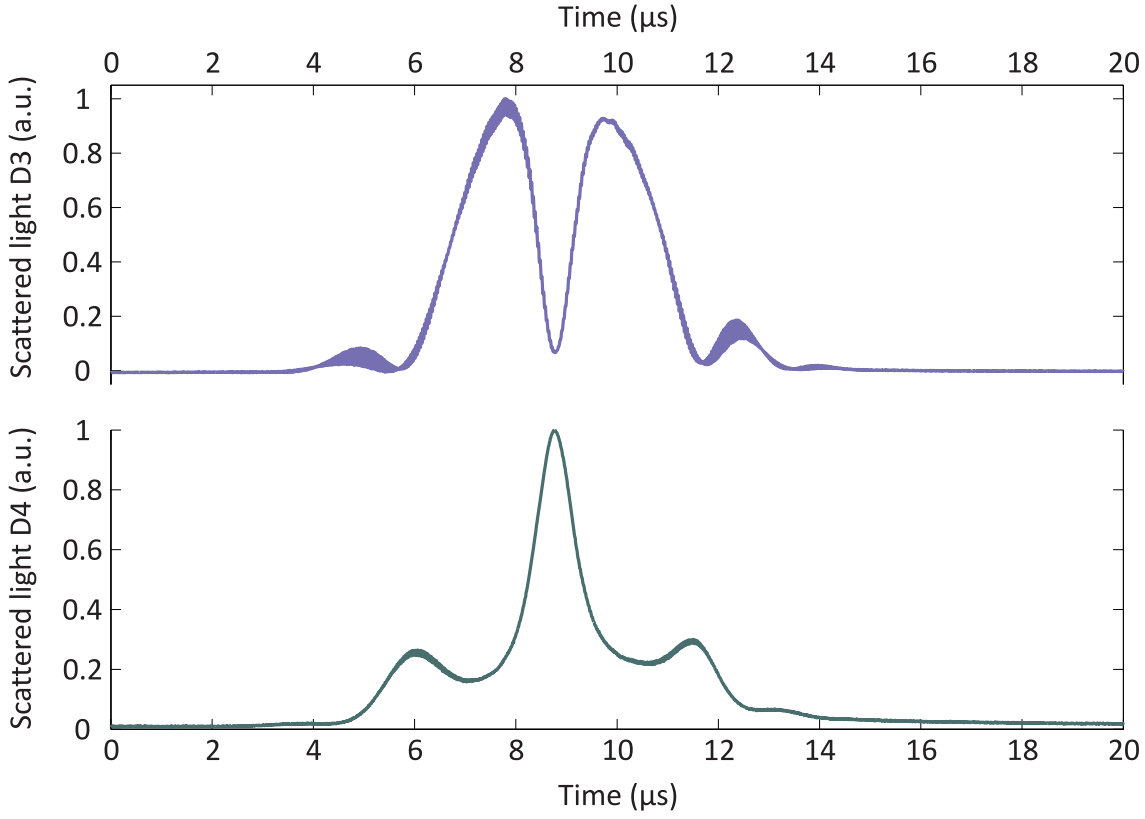


Figure 4.7: Scattering signal from an effective low-field seeker ($\text{TPPF}_{20-x+17x}$ droplet) measured by detectors D3 & D4 (see fig. 3.12). The light detected on D3 (upper curve) mainly consists of the dipole part, whereas D4 (lower curve) is dominated by the quadrupole component of the scattered light. The shape of the curves reveals that the center of mass of this droplet is effectively attracted towards a node of the field at which the dipole part of the scattered light is minimal and the quadrupole part is maximal.

4 Results

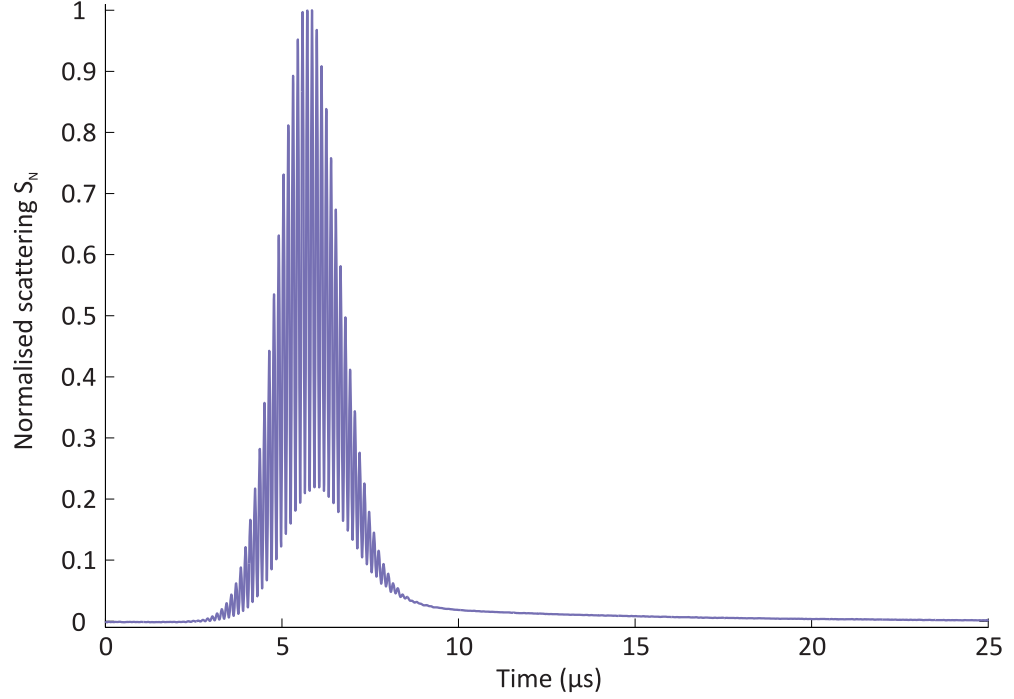


Figure 4.8: Asymmetry in the scattering signal of a $\text{TPPF}_{20-x+17x}$ droplet. As discussed in the main text, this behaviour cannot be explained solely by cooling effects.

of the standing wave. There, the quadrupole component of its scattered light reveals a maximum, whereas the dipole part is minimal.

From the shape of the scattering signal plotted in figure 4.7, we can conclude the following: When the particle crosses the mode, trapping takes place in a region, at which the dipole part of the scattered light is minimal and the quadrupole component shows a maximum. Thus, as explained in section 2.2, we can conclude that in contrast to the particle shown in figure 4.3, this droplet behaves as an effective low-field seeker.

Additionally, one can observe a beating signal on both scattered light curves. It exhibits a frequency of about 30 MHz and thus originates from the particle scattering light from both the TEM_{00} and the TEM_{11} mode when it travels over these regions at which they overlap.

4.5 Asymmetries in the scattered light

Some of the droplets we observe show an unexpected behaviour that has not been fully understood yet. In figure 4.8 the particle's normalised scattering signal S_N is plotted.

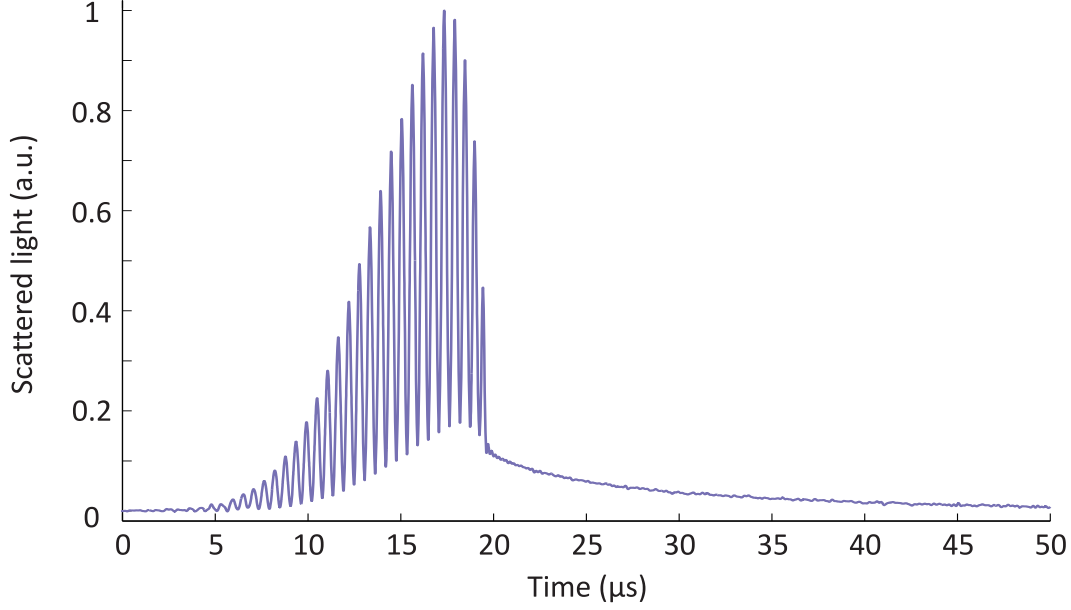


Figure 4.9: $\text{TPPF}_{20-x+17x}$ droplet revealing a sudden change in its scattering behaviour.

It reveals a clear asymmetry, which at first sight seems to be an indicator for slowing effects to take place. However, there are two contradicting arguments:

As already discussed before, the wiggles on the curve correspond to the particle's coupling to the standing wave. The asymmetric part of the curve however seems to be caused by light that does not show these wiggles and thus does not originate from the standing wave. We also have not been able to obtain similar trajectories in our simulations.

One possible model for explaining this behaviour could be the following: As we are dealing with huge intra-cavity powers of up to 25 kW and big droplets exhibiting a high coupling frequency of a few cavity line-widths, there is a lot of light scattered by the particles. Some of it will also be scattered into higher order transversal modes, although they are far detuned from resonance. Therefore, when the droplet travels through these regions, it again scatters this light, some of it onto the detector and some of it in even higher order transversal modes.

In other words, the particle carries some part of the light inside the cavity along its trajectory and scatters it constantly. In this case we could still see the particle on our scattered light detectors although it does not couple to the fundamental cavity mode any more. This effect could lead to an asymmetry in the scattered light as we observe

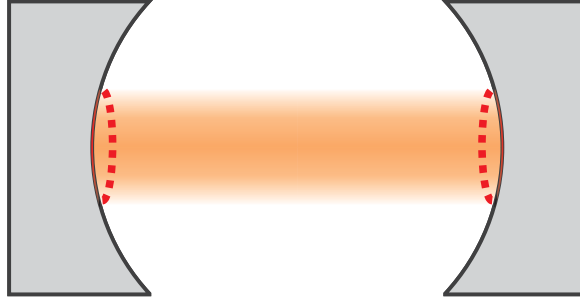


Figure 4.10: Scheme of the thermal effect on the mirrors. Some of the intra-cavity light is absorbed by the coating. This leads to the formation of small bulges which decrease the length of the cavity.

it. Furthermore, the asymmetric shape may also be explained by deformations of the droplets, which may be caused by the cavity field. In order to prove these different models, further calculations and simulations still need to be carried out.

4.6 Sudden changes in the scattering behaviour

As plotted in figure 4.9, some of the droplets show an abrupt change in their scattering signal. Suddenly the modulation caused by their interaction with the standing wave vanishes. This behaviour may be explained as follows:

The intense intra-cavity fields may suffice to change the shape of the droplets or even destroy them totally. Due to absorption they may heat up and evaporate in all directions. In this case they will spread over the standing wave and no wiggles will be seen on the scattered light any more since they average out. These considerations are supported by the following observation:

The fraction of droplets exhibiting such a scattering behaviour could be minimised by lowering the power of the evaporation laser and thus by producing them internally colder from the very beginning.

4.7 Thermal feedback

It has already been mentioned that we observe a thermally induced feedback mechanism which limits the radial cooling effects for slow particles in the set-up presented in this thesis. The effect can be described basically in the following way:

As we scan the piezo voltage and thus steadily increase the length of the cavity, light is coupled into the fundamental mode as soon as we get closer to its resonance. For a

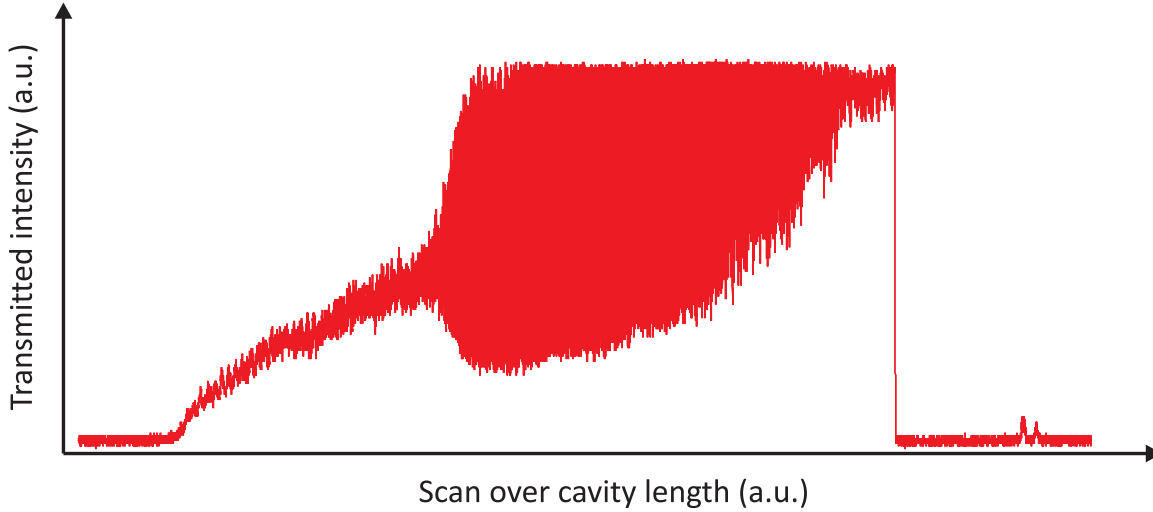


Figure 4.11: Thermally induced broadening of the cavity transmission line for the TEM_{00} mode. The small peaks on the right side correspond to the TEM_{10} & TEM_{01} mode respectively.

finite absorption in the coating of the cavity mirrors, they heat up locally and form a small bulge at the mode center. As depicted in figure 4.10 this leads to a reduction of the cavity length which counteracts the effect of the piezo. In other words, in this self stabilizing region the cavity automatically corrects for deviations and drifts in length. This results in a broadening of the transmission line of the fundamental cavity mode, which can be seen in figure 4.11.

If one scans the cavity length reversely, the opposite happens: The thermal behaviour pushes the cavity over its resonance leading to a transmission peak that is narrower than the expected Lorentzian shape. The system therefore can be called bistable.

For our experiment it has the following consequence: In order to perform cavity cooling we need the particles to shift the cavity towards resonance and thus switch on the field inside the resonator. The thermal feedback however suppresses this rise in intensity and in this way counteracts the cooling mechanism for the droplets.

In order to further characterise the effect, we have simulated the case of a particle passing through the cavity by doubling the pump intensity externally. For this purpose we put a Pockels-cell, which is capable of rotating the polarisation of the light, together with a polarising beam splitter into the pump beam line. This allows us to switch the polarisation and thus the amount of light transmitted through the PBS on a fast timescale. In this way we doubled the pump intensity for $15\ \mu\text{s}$ with an optical rise time of the order of a few nanoseconds.

4 Results

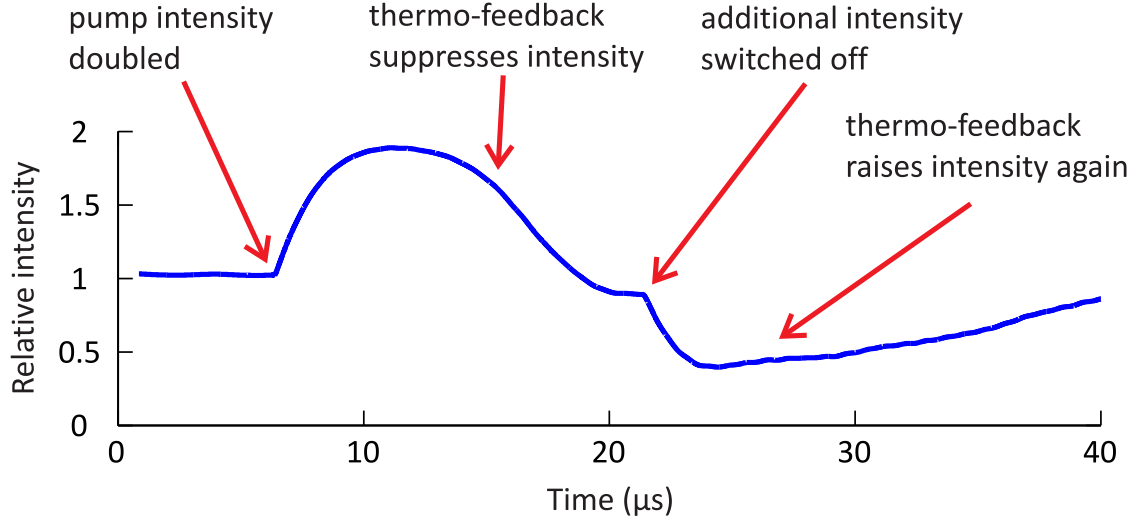


Figure 4.12: Measurement for characterising the time-scale of the thermal feedback.

The results can be seen in figure 4.12. About $5\ \mu\text{s}$ after triggering the Pockels-cell the intensity inside the cavity has reached its maximum. Contrary to one's expectation this maximum does not reach a value of twice the initial intensity since it is already suppressed by the thermo-feedback. Subsequently, the intensity is suppressed further such that after another $7.5\ \mu\text{s}$ it is already less than before switching on the Pockels cell. When the additional power is switched off again after $15\ \mu\text{s}$, it takes the cavity more than $20\ \mu\text{s}$ to recover its initial intensity.

Furthermore, as the scan over the cavity length in figure 4.11 reveals, the system starts to oscillate excessively when the intra-cavity power exceeds a certain value, whereas the magnitude of this limit varied from one measurement run to another. Due to these large self-driven oscillations presented above the thermal feedback limits the maximal intra-cavity power at which we are able to perform our measurements.

We also examined the characteristics of these thermally induced oscillations. In figure 4.13 their frequency power spectrum is plotted. In order to obtain it, we lock the cavity and record the transmitted intensity at two different pump powers: One slightly below and the other a bit above the critical power. At lower pump powers, the thermal oscillator is not driven and shows an FWHM linewidth of about 300 Hz. If one slightly exceeds the critical pump power, the thermal oscillator is driven at 27 kHz and the spectrum shows a sharp oscillation peak with an FWHM linewidth of roughly 1 Hz.

Similar effects have also been reported for different cavity systems: In the group of John Hall they filled a Fabry-Perot cavity (finesse of a few hundred) with 20 torr acety-

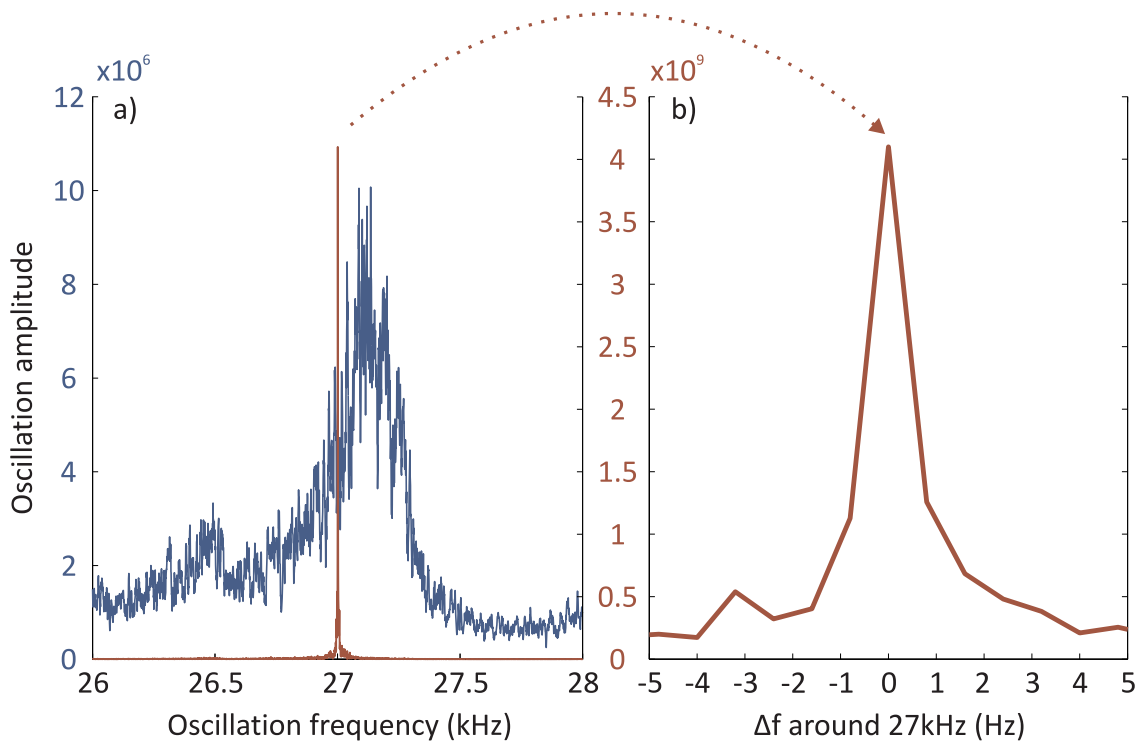


Figure 4.13: (a) Fourier-spectrum of the transmitted intensity for a lower (blue) and a slightly higher (red) pump power. During this measurement the cavity is blue detuned with respect to the laser frequency. For a low pump the thermal oscillator is not driven (FWHM linewidth ≈ 300 Hz). At a higher power, the transmitted intensity exhibits a sharp oscillation peak at 27 kHz. Its width of around 1 Hz is depicted in (b).

4 Results

lene gas [43]. It was optically pumped with 140 mW by a titanium:sapphire laser, tuned to a rotational transition of the gas near 790 nm. In this way, the laser power was converted into heat by the weakly absorbing medium. This caused a change of the gas density and of the refractive index which resulted in a self-locking behaviour very similar to the ones we observe:

In their set-up they obtained a broadening of the transmission line, which led to a self-locking of the cavity to a free running laser. This took place on a time-scale of 100 s, which was normally less than a second. Additionally, in the domain of strong self-tuning they observed oscillations with several sharp frequencies which could be linked to the acoustic boundary conditions of their cell geometry. Finally they wrote: *"The self-locking phenomenon described here is not limited to acetylene or oxygen as an absorber. Whenever heating can cause a change in the optical path of a resonator, self-locking should be expected. An interesting example, observed in our laboratory, is that of a super-highfinesse cavity ($F > 10\,000$) capable of building up a modest laser power, say, 100 mW, into 100 W. The infinitesimal fraction of power absorbed by the low-loss mirrors turned out to be significant with such high circulating powers, causing observable self-locking."* [43]

Also in the group of Kerry J. Vahala they demonstrated thermal self-stability of microcavities both experimentally and theoretically [44].

Finally it should also be mentioned, that we observe the thermal effects to take place very locally. The frequency shift between the TEM_{00} and the TEM_{11} mode shows a clear dependency on the intra-cavity power, which indicates that the weakly pumped higher order mode is affected significantly less by the thermal effects than the strongly pumped fundamental mode. This observation was further affirmed in the following experiment:

On a fast time-scale we lock the laser frequency onto the cavity by using a higher order TEM mode as reference signal. Then we monitor the transmitted intensity through the fundamental mode, which is intensely pumped by a frequency shifted beam. When the pump power of the fundamental mode exceeds a critical level its transmitted intensity shows an oscillatory behaviour although the cavity is perfectly stable for the higher order mode.

5 Conclusion & Outlook

In this thesis we have presented an experimental set-up, which features the interaction of strongly enhanced infra-red light with molecular droplets. They have been produced in a novel evaporation scheme. The measured results affirm, that the modes in a resonator provide a way to characterise the properties of the droplets as well as information about their trajectory through the cavity.

Furthermore, we were able to observe first mechanical effects of light on molecular nano-droplets in a cavity. On one hand they lead a way towards cavity cooling of dielectric particles: We observe the cavity induced turning back of a droplet transiting the cavity - a consequence of a particle interacting with a non-conservative potential.

We further have demonstrated the effective low-field seeking behaviour of droplets, which exceed a critical size that is given by the structure of the standing wave. Throughout these measurements, via monitoring phase & amplitude of the cavity field and the scattering pattern of the particles with two orthogonally placed detectors, we gain an insight into both the cavity and particle dynamics as well as the scattering behaviour of the droplets. Through our digitizer system we obtain fully time-resolved signals with high resolutions.

In the course of this thesis, we have discussed the prospects for manipulating the radial part of the velocities for particles transiting a strongly pumped and detuned cavity mode. Simulations of the system indicate a capability of this scheme to trap and cool particles radially. However, the current system is limited by the discussed thermal feedback effect. Hence, in order to reach the radial cooling regime, one needs to circumvent this limitation.

One way seems to be paved by looking at effects, which take place on a faster timescale than the thermal feedback. In this case one may introduce a fast second feedback loop in addition to the piezo transducer. A double-passed AOM in the main beam path should be capable of stabilising the pump frequency onto the thermally induced fluctuations in the cavity length and thus keep the cavity field free from driven thermal oscillations.

For these reasons, such a set-up would have to focus on cooling the motion along the

5 Conclusion & Outlook

standing wave axis in a Sisyphus type mechanism. But in this case one has to reconsider the scaling of the particle's coupling to the cavity. In the radial cooling scheme, the particle size is only limited by its scattering and hence a lack of coupling can be compensated by an increasing droplet size.

In contrast to that, for cooling the transverse motion of a particle, its size limit is mainly dominated by the structure of the standing wave. As it was discussed, with growing radii of the droplets the transverse force is steadily reduced and can even fall below zero. This results in an effective low-field seeking behaviour of the particles.

Since most of the droplets that we observe are too big, they are not suitable for these future experiments. Therefore, different particle sources are needed which are capable of launching smaller particles with lower velocities. In order to maintain a high field coupling even for small particles the finesse of the cavity should also be increased further. Additionally it is beneficial to work with particles that exhibit a higher polarizability over mass ratio.

For these purposes, different launching schemes for different nanoparticles of compatible optical properties are currently being explored. These tests range from laser induced acoustic desorption (LIAD) mechanisms [45–47] to matrix assisted laser evaporation schemes and other related procedures [48]. Possible candidates may be nanoparticles made up of Boron Nitride, Nano-Diamonds, Silicon or Silicon Carbide since they show the most promising values for α/m whereas their absorption is low. Fluorescent nano-spheres may also be advantageous for testing the various sources, since they can be detected by laser induced fluorescence methods.

As described, the basic scheme for the transverse cooling works as follows. The nanoparticles should be launched through the resonator. In this way, while they transect the fundamental mode, their transverse kinetic energy can be cooled through the field dynamics. This configuration demands a particle source, which produces intrinsically slow particles. Their forward velocities need to be low enough in order to obtain long interaction times with the cavity field. Furthermore the particle motion in direction of the standing wave needs to be sufficiently slow for the following reason:

Cavity cooling in this Sisyphus scheme works best for transverse velocities of $kv \approx \kappa$. In this case, the cavity field reacts in a most efficient way to the particle position. The detuning is optimally set to $\Delta = -\kappa$ since in this case the field intensity reacts in a most pronounced way to a change in cavity phase. For typical cavity linewidths this results in optimal transverse velocities of approximately 0.5 m s^{-1} .

A limiting factor for the cooling in cavity axis is given by the finite interaction time, which originates from the fact that the particle transits the mode. In order to increase

this interaction time one can think about trapping the particles radially. This can be achieved by applying active optical feedback. The distinctness of the scattered light, which we are able to detect, may therefore be used as trigger in order to switch the pump intensity in a similar way to the experiments in the group of L. Novotny and M. Raizen [7, 17].

Although in this way the interaction time may be extended, the cooling rate for the transverse velocity will drop constantly for the following reason: As soon as the transverse kinetic energy falls below the optical potential of the standing wave a particle gets trapped in an anti-node of the mode. In this case it is bound to regions of similar coupling. Hence, the energy loss per cycle decreases as the particle gets trapped deeper.

One could think of counteracting this effect by lowering the intra-cavity intensity and thus flattening the standing wave potential. Although this allows the particles to run over the standing wave freely at lower velocities, it also decreases the friction force of the cooling process in the same manner.

The following modification of the set-up, which was proposed by S. Habraken et al. [49] may increase the cooling rate of the scheme. Pumping a second fundamental cavity mode, which is separated by a free spectral range, results in a cancellation of the optical potential in the center of the cavity. In this case, the resulting dynamics is almost purely dissipative. In other words, in this two-mode scheme the optical potential can be compensated locally and the velocities at which the particle is trapped by the standing wave can be reduced by almost two orders of magnitude.

By all these modifications, substantial cooling of a nano-particle's transverse velocity should be within reach.

Finally, as mentioned at the beginning of the thesis, future quantum experiments will additionally require the nano-particles to be sufficiently cold internally. For that purpose it will be interesting to consider extending the source in the following way. The particles may be first mass-selected and cooled in a cryogenic ion trap to temperatures around 4 K before they are neutralised and coupled to a cavity.

If one achieves to accommodate all these demands and obtain a collimated beam of slow nano-particles in forward direction, it can be considered to design an interferometer set-up on top in a fountain configuration. It may also be a promising starting point for future experiments under micro-gravity [50].

6 Supplements

6.1 Molecules

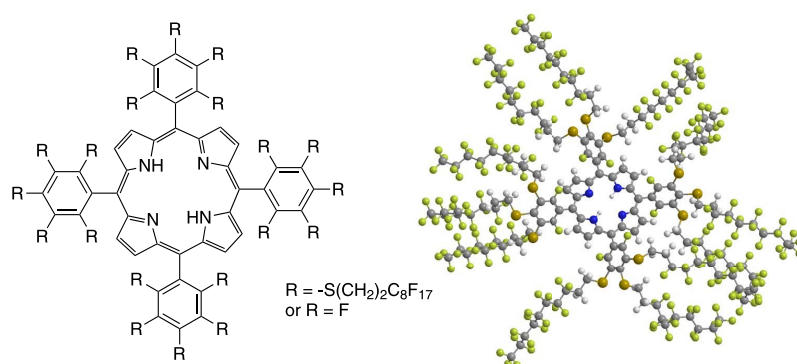


Figure 6.1: 2D structural formula of TPPF_{20-x+17x} (left). The value of x determines the amount of fluorinated side chains. The 3D structure is depicted for $x = 12$ (right). It exhibits a mass of 6494 amu.

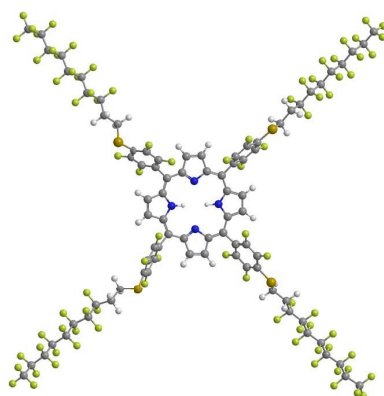


Figure 6.2: 3D structural formula of TPPF₈₄. This molecule exhibits a mass of 2814 amu.

6 Supplements

In both figures 6.1 & 6.2 the colours represent the following atoms: Gray - C, White - H, Blue - N, Yellow - S and Green - F.

6.2 Extracting phase and amplitude of the TEM₀₀ & TEM₁₁ mode from the digitized beating signal

```
%Beating signal is saved under 'ac.bin'

fid=fopen('ac.bin');
AC=single(fread(fid,'single'));
fclose(fid);

                                %Data loaded into workspace

AC=fft(AC);

                                %Fourier transform

[~,freq60]=max(abs(AC(7E7:8E7)));
                                %Find peak of beating for fundamental mode
                                %Position in fourier spektrum 60 MHz <-> 7.5E7

[~,freq90]=max(abs(AC(1.05E8:1.2E8)));
                                %Find peak of beating for TEM11 mode
                                %Position in fourier spektrum 90 MHz <-> 1.125E8

freq60=freq60+7E7-1;
freq90=freq90+1.05E8-1;

bandwidth=round((freq90-freq60)/2);
                                %Calculated bandwidth for fundamental mode such that there
                                %is no overlap with the TEM11 mode

bandwidth1=1.25E8-freq90-1;
                                %Set maximal bandwidth for TEM11 mode

%Start calculating phases:
%Peaks of fundamental and TEM11 mode are shifted to zero respectively
%and so are the regions within the bandwidths accordingly

AC60(1:bandwidth+1)=AC(freq60:freq60+bandwidth);
AC60(bandwidth+2:2*bandwidth+2)=AC(freq60-bandwidth-1:freq60-1);
```

6.2 Extracting phase and amplitude of the TEM_{00} & TEM_{11} mode from the digitized beating signal

```
AC90(1:bandwidth1+1)=AC(freq90:freq90+bandwidth1);
AC90(bandwidth1+2:2*bandwidth1+2)=AC(freq90-bandwidth1-1:freq90-1);

clear AC;

%Remaining parts are set to zero

j=2.5E8-length(AC60);
j1=2.5E8-length(AC90);

AC60=[AC60(1:bandwidth+1),zeros(1,j),AC60(bandwidth+2:2*bandwidth+2)];
AC60=ifft(AC60);

%Calculating phase and amplitude for fundamental mode

phase_00=angle(AC60);
amplitude_00=abs(AC60);

clear AC60;

AC90=[AC90(1:bandwidth1+1),zeros(1,j1),AC90(bandwidth1+2:2*bandwidth1+2)];
AC90=ifft(AC90);

%Calculating phase and amplitude for TEM11 mode

phase_11=angle(AC90);
amplitude_11=abs(AC90);

clear AC90;

%Unwrap and filter (high-pass > 40Hz) for both phases

phase_00=unwrap(phase_00);

phase_00=fft(phase_00);
phase_00(1:50)=0;
phase_00=ifft(phase_00,'symmetric');

phase_11=unwrap(phase_11);

phase_11=fft(phase_11);
phase_11(1:50)=0;
phase_11=ifft(phase_11,'symmetric');
```

6.3 Reconstruction of the trajectory for a particle trapped in the standing wave

```
%scatt --> filtered \& normalised scattered light from detector D3
%yfit --> Gaussian fit of scattered light

pos=scatt./yfit;                                %Scattered light divided by Gaussian envelope
                                                %only coupling to standing wave remains

[a,b]=findpeaks(double(scatt),'MINPEAKDISTANCE',170);
                                                %Positions b of Maxima in scattered light
[c,d]=findpeaks(double(-scatt),'MINPEAKDISTANCE',170);
                                                %Positions d of Minima in scattered light

                                                %From b(3) to b(6) the particle is untrapped
                                                %From b(6) to b(11) the particle is trapped
                                                %From b(11) to b(13) the particle is untrapped

x=[];

for i=3:5;                                       %Running over standing wave
    xa=[];
    xa=[xa,real(acos(sqrt(pos(b(i)+1:d(i)))))+(i-2)*pi/2 ...
        %Basic reconstruction for Max to Min
        -real(acos(sqrt(pos(b(i)+1)))) ...
        %Corrects beginning
        +(0:d(i)-b(i)-1)...
        *(pi/2-real(acos(sqrt(pos(d(i)))))+real(acos(sqrt(pos(b(i)+1)))) ...
        /(length((0:d(i)-b(i)-1))-1)];
        %Corrects end by linear regression

    xa=[xa,-real(acos(sqrt(pos(d(i)+1:b(i+1)))))+(i)*pi/2 ...
        %Basic reconstruction for Min to Max
        +real(acos(sqrt(pos(d(i)+1))))-pi/2 ...
        %Corrects beginning
        +(0:b(i+1)-d(i)-1)...
        *(real(acos(sqrt(pos(b(i+1)))))+real(acos(sqrt(pos(d(i)+1))))-pi/2) ...
        /(length((0:b(i+1)-d(i)-2))-1)];
        %Corrects end by linear regression

    xa=xa+(i-2)*pi/2;                           %Adds offset for running over standing wave
```


6.3 Reconstruction of the trajectory for a particle trapped in the standing wave

```

x=[x, xa]; %Builds up trajectory vector x
end

x1=x;
clear xa;
clear x;
xb=[];

for i=6:10 %Reconstruction for the trapped motion
    if mod(i,2)== 1
        xb=[xb, real(acos(sqrt(pos(b(i)+1:b(i+1)))))*(mod(i,2)-0.5)*-2 ...
            +real(acos(sqrt(pos(b(i)+1))))+ ...
            (0:b(i+1)-b(i)-1) ...
            *real(acos(sqrt(pos(b(i+1))))-acos(sqrt(pos(b(i)+1)))) ...
            /length((0:b(i+1)-b(i)-1)-1)];
    else
        xb=[xb, real(acos(sqrt(pos(b(i)+1:b(i+1))))*(mod(i,2)-0.5)*-2 ...
            -real(acos(sqrt(pos(b(i)+1)))) ...
            + (0:b(i+1)-b(i)-1) ...
            *real(acos(sqrt(pos(b(i+1))))-acos(sqrt(pos(b(i)+1)))) ...
            /length((0:b(i+1)-b(i)-1)-1)];
    end
end

x2=xb+4*pi; %Adds offset for trapped trajectory to fit to
             %untrapped part x1

x=[];

for i=11:13;
    xa=[];
    xa=[xa, real(acos(sqrt(pos(b(i)+1:d(i)))))+(i-2)*pi/2 ...
        -real(acos(sqrt(pos(b(i)+1)))) ...
        + (0:d(i)-b(i)-1) ...
        * (pi/2-real(acos(sqrt(pos(d(i)))))+real(acos(sqrt(pos(b(i)+1)))) ...
        / (length((0:d(i)-b(i)-1)-1)];

    xa=[xa, -real(acos(sqrt(pos(d(i)+1:b(i+1)))))+(i)*pi/2 ...
        +real(acos(sqrt(pos(d(i)+1))))-pi/2 ...
        + (0:b(i+1)-d(i)-1) ...
        * (real(acos(sqrt(pos(b(i+1))))+real(acos(sqrt(pos(d(i)+1))))-pi/2) ...
        / (length((0:b(i+1)-d(i)-2)))];

    xa=xa+(i-2)*pi/2; %Adds offset for running over standing wave
    x=[x, xa]; %Builds up trajectory vector x
end

```

6 Supplements

```
end

x3=-x+13*pi;                                %Sets direction for running out trajectory
                                              %and adds the offset to fit to trapped curve

traj1=([x1,x2,x3]);                          %Combines all parts of trajectory

%Create standing wave plot

r=linspace(-20000,20000,10000)/529.5;
                                              %Vektor in forward direction (z)
                                              %in units of waists (529.5 from Gaussfit)

s=linspace(0,20,3000)/2/pi;
                                              %Vektor in direction of standing wave (x)
                                              %in units of half the wavelength

prof = cos((s*2*pi).').^2*exp(-(r).^2/(1)^2/2);
                                              %Profile of the standing wave with Gaussian
                                              %envelope

imagesc(r.',s,prof);                        %Plot standing wave
set(gca,'YDir','normal')                    %Set y-axis increasing
colormap('Gray')                            %Set colors to black-white
hold on                                     %Keeps the standing wave as background
plot(((b(3)+1:b(14))-2053+locs(1))/529.5,traj1);
                                              %Plot trajectory with time-offset given by
                                              %the maximum of the Gaussfit and in units of
                                              %cavity waists
```

Bibliography

- [1] K. Hornberger, S. Gerlich, P. Haslinger, S. Nimmrichter, and M. Arndt, “Colloquium: Quantum interference of clusters and molecules,” *Reviews of Modern Physics*, vol. 84, pp. 157–173, Feb. 2012.
- [2] S. Nimmrichter, K. Hornberger, P. Haslinger, and M. Arndt, “Testing spontaneous localization theories with matter-wave interferometry,” *Physical Review A*, vol. 83, p. 043621, Apr. 2011.
- [3] O. Romero-Isart, A. C. Pflanzner, M. L. Juan, R. Quidant, N. Kiesel, M. Aspelmeyer, and J. I. Cirac, “Optically levitating dielectrics in the quantum regime: Theory and protocols,” *Physical Review A*, vol. 83, p. 013803, Jan. 2011.
- [4] S. Nimmrichter and K. Hornberger, “Macroscopicity of Mechanical Quantum Superposition States,” *Physical Review Letters*, vol. 110, p. 160403, Apr. 2013.
- [5] D. E. Chang, C. A. Regal, S. B. Papp, D. J. Wilson, J. Ye, O. Painter, H. J. Kimble, and P. Zoller, “Cavity opto-mechanics using an optically levitated nanosphere,” *Proceedings of the National Academy of Sciences of the United States of America*, vol. 107, pp. 1005–10, Jan. 2010.
- [6] P. Haslinger, N. Dörre, P. Geyer, J. Rodewald, S. Nimmrichter, and M. Arndt, “A universal matter-wave interferometer with optical ionization gratings in the time domain,” *Nature Physics*, vol. 9, pp. 144–148, Feb. 2013.
- [7] T. Li, S. Kheifets, and M. G. Raizen, “Millikelvin cooling of an optically trapped microsphere in vacuum,” *Nature Physics*, vol. 7, pp. 527–530, Mar. 2011.
- [8] S. Eibenberger, S. Gerlich, M. Arndt, J. Tüxen, and M. Mayor, “Electric moments in molecule interferometry,” *New Journal of Physics*, vol. 13, p. 043033, Apr. 2011.
- [9] M. Arndt, T. Juffmann, and V. Vedral, “Quantum physics meets biology,” *HFSP journal*, vol. 3, pp. 386–400, Dec. 2009.

Bibliography

- [10] S. Gerlich, S. Eibenberger, M. Tomandl, S. Nimmrichter, K. Hornberger, P. J. Fagan, J. Tüxen, M. Mayor, and M. Arndt, “Quantum interference of large organic molecules.,” *Nature communications*, vol. 2, p. 263, Jan. 2011.
- [11] T. Hänsch and A. Schawlow, “Cooling of gases by laser radiation,” *Optics Communications*, vol. 13, pp. 68–69, Jan. 1975.
- [12] C. Cohen-Tannoudji, “Manipulating Atoms with Photons,” *Physica Scripta*, vol. T76, no. 1, p. 33, 1998.
- [13] J. Dalibard and C. Cohen-Tannoudji, “Laser cooling below the Doppler limit by polarization gradients: simple theoretical models,” *Journal of the Optical Society of America B*, vol. 6, p. 2023, Nov. 1989.
- [14] M. Kasevich and S. Chu, “Laser cooling below a photon recoil with three-level atoms,” *Physical Review Letters*, vol. 69, pp. 1741–1744, Sept. 1992.
- [15] J. Lawall, F. Bardou, B. Saubamea, K. Shimizu, M. Leduc, A. Aspect, and C. Cohen-Tannoudji, “Two-Dimensional Subrecoil Laser Cooling,” *Physical Review Letters*, vol. 73, pp. 1915–1918, Oct. 1994.
- [16] E. S. Shuman, J. F. Barry, and D. Demille, “Laser cooling of a diatomic molecule.,” *Nature*, vol. 467, pp. 820–3, Oct. 2010.
- [17] J. Gieseler, B. Deutsch, R. Quidant, and L. Novotny, “Subkelvin Parametric Feedback Cooling of a Laser-Trapped Nanoparticle,” *Physical Review Letters*, vol. 109, p. 103603, Sept. 2012.
- [18] P. Horak, G. Hechenblaikner, K. Gheri, H. Stecher, and H. Ritsch, “Cavity-Induced Atom Cooling in the Strong Coupling Regime,” *Physical Review Letters*, vol. 79, pp. 4974–4977, Dec. 1997.
- [19] V. Vuletić and S. Chu, “Laser Cooling of Atoms, Ions, or Molecules by Coherent Scattering,” *Physical Review Letters*, vol. 84, pp. 3787–3790, Apr. 2000.
- [20] B. Lev, A. Vukics, E. Hudson, B. Sawyer, P. Domokos, H. Ritsch, and J. Ye, “Prospects for the cavity-assisted laser cooling of molecules,” *Physical Review A*, vol. 77, p. 023402, Feb. 2008.
- [21] M. Gangl, P. Horak, and H. Ritsch, “Cooling neutral particles in multimode cavities without spontaneous emission,” *Journal of Modern Optics*, vol. 47, no. 14/15, pp. 2741–2753, 2000.

- [22] S. Nimmrichter, K. Hammerer, P. Asenbaum, H. Ritsch, and M. Arndt, “Master equation for the motion of a polarizable particle in a multimode cavity,” *New Journal of Physics*, vol. 12, p. 083003, Aug. 2010.
- [23] P. Maunz, T. Puppe, I. Schuster, N. Syassen, P. W. H. Pinkse, and G. Rempe, “Cavity cooling of a single atom,” *Nature*, vol. 428, pp. 50–2, Mar. 2004.
- [24] S. Nuß mann, K. Murr, M. Hijkema, B. Weber, A. Kuhn, and G. Rempe, “Vacuum-stimulated cooling of single atoms in three dimensions,” *Nature Physics*, vol. 1, pp. 122–125, Oct. 2005.
- [25] A. Boozer, A. Boca, R. Miller, T. Northup, and H. Kimble, “Cooling to the Ground State of Axial Motion for One Atom Strongly Coupled to an Optical Cavity,” *Physical Review Letters*, vol. 97, pp. 2–5, Aug. 2006.
- [26] M. Wolke, J. Klinner, H. Keß ler, and A. Hemmerich, “Cavity cooling below the recoil limit,” *Science (New York, N.Y.)*, vol. 337, pp. 75–8, July 2012.
- [27] M. H. Schleier-Smith, I. D. Leroux, H. Zhang, M. A. Van Camp, and V. Vuletić, “Optomechanical Cavity Cooling of an Atomic Ensemble,” *Physical Review Letters*, vol. 107, p. 143005, Sept. 2011.
- [28] N. Kiesel, F. Blaser, U. Delic, D. Grass, R. Kaltenbaek, and M. Aspelmeyer, “Cavity cooling of an optically levitated nanoparticle,” *arXiv preprint arXiv:1304.66792v2 [quant-ph]*, p. 14, Apr. 2013.
- [29] P. F. Barker, “Cavity cooling of an optically trapped nanoparticle,” *Physical Review A*, vol. 81, pp. 1–6, Feb. 2010.
- [30] H. Mabuchi, Q. A. Turchette, M. S. Chapman, and H. J. Kimble, “Real-time detection of individual atoms falling through a high-finesse optical cavity,” *Optics letters*, vol. 21, pp. 1393–5, Sept. 1996.
- [31] T. Puppe, P. Maunz, T. Fischer, P. Pinkse, and G. Rempe, “Single-Atom Trajectories in Higher-Order Transverse Modes of a High-Finesse Optical Cavity,” *Physica Scripta*, vol. T112, no. 1, p. 7, 2004.
- [32] T. W. Lynn, K. Birnbaum, and H. J. Kimble, “Strategies for real-time position control of a single atom in cavity QED,” *Journal of Optics B: Quantum and Semiclassical Optics*, vol. 7, pp. S215–S225, Oct. 2005.
- [33] O. F. Mossotti, *Mem. di mathem. e fisica in Modena*. 24 11 ed., 1850.

Bibliography

- [34] S. Nimmrichter. PhD thesis, 2013.
- [35] A. C. Pflanze, O. Romero-Isart, and J. I. Cirac, “Master-equation approach to optomechanics with arbitrary dielectrics,” *Physical Review A*, vol. 86, p. 013802, July 2012.
- [36] P. Asenbaum, “Towards cavity cooling of a molecular beam,” diplomarbeit, 2009.
- [37] E. A. Donley, T. P. Heavner, F. Levi, M. O. Tataw, and S. R. Jefferts, “Double-pass acousto-optic modulator system,” *Review of Scientific Instruments*, vol. 76, no. 6, p. 063112, 2005.
- [38] P. Asenbaum and M. Arndt, “Cavity stabilization using the weak intrinsic birefringence of dielectric mirrors,” *Optics Letters*, vol. 36, p. 3720, Sept. 2011.
- [39] R. W. P. Drever, J. L. Hall, F. V. Kowalski, J. Hough, G. M. Ford, A. J. Munley, and H. Ward, “Laser phase and frequency stabilization using an optical resonator,” *Applied Physics B Photophysics and Laser Chemistry*, vol. 31, pp. 97–105, June 1983.
- [40] J. Helmcke, S. A. Lee, and J. L. Hall, “Dye laser spectrometer for ultrahigh spectral resolution: design and performance,” *Applied Optics*, vol. 21, p. 1686, May 1982.
- [41] J. Tüxen, S. Eibenberger, S. Gerlich, M. Arndt, and M. Mayor, “Highly Fluorous Porphyrins as Model Compounds for Molecule Interferometry,” *European Journal of Organic Chemistry*, pp. 4823–4833, July 2011.
- [42] T. Juffmann, A. Milic, M. Müllneritsch, P. Asenbaum, A. Tsukernik, J. Tüxen, M. Mayor, O. Cheshnovsky, and M. Arndt, “Real-time single-molecule imaging of quantum interference,” *Nature nanotechnology*, vol. 7, pp. 297–300, May 2012.
- [43] P. Dubé, L. Ma, J. Ye, P. Jungner, and J. Hall, “Thermally induced self-locking of an optical cavity by overtone absorption in acetylene gas,” *JOSA B*, vol. 13, no. 9, pp. 2041–2054, 1996.
- [44] T. Carmon, L. Yang, and K. Vahala, “Dynamical thermal behavior and thermal self-stability of microcavities,” *Optics express*, vol. 12, pp. 4742–50, Oct. 2004.
- [45] A. V. Zinovev, I. V. Veryovkin, J. F. Moore, and M. J. Pellin, “Laser-driven acoustic desorption of organic molecules from back-irradiated solid foils,” *Analytical chemistry*, vol. 79, pp. 8232–41, Nov. 2007.

- [46] A. Zinovev, I. Veryovkin, and M. Pellin, *Acoustic Waves - From Microdevices to Helioseismology*. InTech, Nov. 2011.
- [47] A. M. Dow, A. R. Wittrig, and H. I. Kenttämää, “Laser-induced acoustic desorption (LIAD) mass spectrometry,” *European journal of mass spectrometry (Chichester, England)*, vol. 18, pp. 77–92, Jan. 2012.
- [48] Z. R. Du, N. Palina, J. Chen, A. Aberle, B. Hoex, and M. H. Hong, “Enhancement of laser-induced rear surface spallation by pyramid textured structures on silicon wafer solar cells,” *Optics Express*, vol. 20, p. A984, Nov. 2012.
- [49] S. J. M. Habraken, W. Lechner, and P. Zoller, “Resonances in dissipative optomechanics with nanoparticles: Sorting, speed rectification, and transverse cooling,” *Physical Review A*, vol. 87, p. 053808, May 2013.
- [50] G. Amelino-Camelia, K. Aplin, M. Arndt, J. D. Barrow, R. J. Bingham, C. Borde, P. Bouyer, M. Caldwell, a. M. Cruise, T. Damour, P. DâĂŽArrigo, H. Dittus, W. Ertmer, B. Foulon, P. Gill, G. D. Hammond, J. Hough, C. Jentsch, U. Johann, P. Jetzer, H. Klein, A. Lambrecht, B. Lamine, C. Lämmerzahl, N. Lockerbie, F. Loeffler, J. T. Mendonca, J. Mester, W.-T. Ni, C. Pegrum, A. Peters, E. Rasel, S. Reynaud, D. Shaul, T. J. Sumner, S. Theil, C. Torrie, P. Touboul, C. Trenkel, S. Vitale, W. Vodel, C. Wang, H. Ward, and A. Woodgate, “GAUGE: the GrAnd Unification and Gravity Explorer,” *Experimental Astronomy*, vol. 23, pp. 549–572, June 2008.

Curriculum Vitae

Personal Information

Name	Stefan Kuhn
Date and place of birth	4.10.1987, Vienna
Citizenship	Austrian
Languages	German (native), English (fluently), Spanish (basics)

Educational History

Since October 2011	Master thesis in the group of Prof. Dr. Markus Arndt
March 2011- July 2013	Master studies of Physics at the University of Vienna
March 2011	Bachelor of Science degree from the University of Vienna
March 2007- March 2011	Study of Physics at the University of Vienna
March 2007- June 2007	Study of Chemistry at the University of Vienna
September 2006- February 2007	Compulsory military service in the Austrian army
1998-2006	High school at the Albertus-Magnus-Gymnasium in Vienna

Vienna, July 2013